SEDIMENTOLOGY the journal of the International Association of Sedimentologists

Sedimentology (2022) doi: 10.1111/sed.12969

Compositional, micromorphological and geotechnical characterization of Holocene Tiber floodplain deposits (Rome, Italy) and sequence stratigraphic implications

DANIEL TENTORI* , MARCO MANCINI* , SALVATORE MILLI*,† , FRANCESCO STIGLIANO* , SIMONE TANCREDI† and MASSIMILIANO MOSCATELLI*

**Istituto di Geologia Ambientale e Geoingegneria (IGAG), Consiglio Nazionale delle Ricerche, Via Salaria km 29, Montelibretti, 300 – 00015, Italy (E-mail: daniel.tentori@igag.cnr.it)*

†Dipartimento di Scienze della Terra, SAPIENZA Università di Roma, Piazzale Aldo Moro 5, Roma, 00185, Italy

Associate Editor – Nathan Sheldon

ABSTRACT

This study reports a high-resolution micromorphological characterization of floodplain deposits to investigate the relationships among compositional, textural and geotechnical data, and integrate soil micromorphology with sequence stratigraphy. Compositional and textural characterization of facies associations and soil features are calibrated against geotechnical parameters. The latter, obtained from cone penetration and pocket penetrometer tests from a borehole advanced 60 m into the Tiber channel belt and floodplain, show that depositional features and post-depositional modifications are intrinsically associated with cone penetration test parameters: cone resistance; sleeve friction; and friction ratio. Petrographic and micromorphological features document pedogenetic modifications across stratigraphic markers evidenced by faunal and plant activity, accumulation of peat, and typified by precipitation of heavy metals, iron oxides and secondary carbonates. All of these features developed in correspondence with alluvial flooding surfaces that are correlated with non-marine and marine flooding surfaces recognized in the transgressive and highstand coastal and lagoonal deposits of the Tiber Depositional Sequence. These observations may serve as a model to reconstruct the sequence-stratigraphic evolution of ancient relict soils. Nevertheless, additional criteria (for example, their stratigraphic position and correlative surfaces) are necessary to adequately interpret the genesis of such low-rank stratigraphic surfaces. This work demonstrates that a combination between sedimentological and stratigraphic observations and soil micromorphology can be critical to supplement field observations and determine the relative effect of pedogenic and depositional processes on the organization, composition and texture, and geotechnical properties of floodplain in urban areas.

Keywords Flooding surfaces, floodplain, geotechnical parameters, micromorphology, palaeosols, sequence-stratigraphy, Tiber River, Upper Pleistocene–Holocene.

INTRODUCTION

Floodplains areas are highly sensitive to changes in sediment discharge and accommodation space and record a complex depositional history that reflects allogenic processes, including climate and base-level changes, and local autocyclic processes (Kraus, 1987; Blum *et al.*, 1994; McCarthy & Plint, 1998; Blum & Törnqvist, 2000; Allen, 2008; Romans *et al.*, 2016). Depositional hiatuses occurring in these deposits, record physical and chemical modifications caused by pedogenesis, a process influenced by changes in water table and rainfall rates, weathering and biological activity (Retallack, 2001). This complexity is expressed by a high vertical and lateral facies variability and results in a significant textural and compositional heterogeneity of floodplain deposits. Thus, developing reliable models to predict the ancient stratigraphic architecture of alluvial plains and palaeovalleys can be very challenging. In this respect, Quaternary depositional systems, and especially the ones developed in the Holocene, offer well-preserved archives where the response of local factors to the external and internal forcing can be linked to high-resolution stratigraphic records.

Non-marine Quaternary successions have been recently investigated to describe and document palaeosol–channel belt stratigraphic relationships to interpret their development at a basin scale (Blum & Törnqvist, 2000; Blum *et al.*, 2013; Amorosi *et al.*, 2017). This is of great value for sequence-stratigraphic studies but has the inevitable downside of overlooking facies variability at the mesoscale and microscale. In this regard, palaeosol micromorphology deserves closer attention as it provides indications with respect to the duration of non-deposition and the degree of soil development (McCarthy & Plint, 1998), and thereby can be employed to recognize major and minor stratigraphic markers (for example, sequence boundaries, maximum flooding surfaces, parasequence boundaries, transgressive and non-marine flooding surfaces; Blum & Price, 1998; Blum & Törnqvist, 2000; Diessel, 2007; Srivastava *et al.*, 2010; Jerrett *et al.*, 2011; Milli *et al.*, 2016; Srivastava *et al.*, 2018; Zuffetti *et al.*, 2018; Amorosi *et al.*, 2021). Although the use of petrographic procedures to characterize compositional variations within chronostratigraphic units and across stratigraphic unconformities has been applied in sand provenance studies (e.g. Zuffa *et al.*, 1995; Amorosi & Zuffa, 2011; Tentori *et al.*, 2016, 2018; Tentori *et al.*, 2021), a clear understanding of its application to characterize the soil chronosequence within depositional sequences needs more careful scrutiny (see Blum & Törnqvist, 2000).

This study focuses on mesoscopic and microscopic sedimentological description of floodplain deposits and their associated palaeosols by integrating micromorphological and petrographic analyses to demonstrate that soil micromorphology is an essential prerequisite for the reconstruction of palaeoenvironmental settings and to investigate post-depositional soil transformations. For this purpose, sedimentological, stratigraphic and pedological observations from a core (60 m depth) into the Tiber Holocene floodplain succession in Rome were combined. A detailed micromorphological characterization of the deposits through petrographic, X-ray diffraction (XRD) and scanning electron microscopy (SEM) analysis was carried out to investigate the processes accountable for the genesis of pedogenetic features. Sediment provenance and soil micromorphology were used in combination to reconstruct the mutual cause−effect relationship regulating detrital and authigenic mineral composition and texture, and to determine the relative effect of pedogenic and geological processes on floodplain deposits organization, composition and texture. Lastly, micromorphological features are used to characterize incipient palaeosols that developed in correspondence with alluvial flooding surfaces traced across a selected sector the Holocene Tiber alluvial plain and that should correspond with the marine and non-marine flooding surfaces recognized in the transgressive coastal and lagoonal deposits of the Tiber Depositional Sequence (TDS). Therefore, this study proves that a combination between sedimentological and stratigraphic observations and soil micromorphology can be critical to supplement employed field observations and stratigraphic methods (see also McCarthy & Plint, 1998).

Our case study offers the opportunity to anchor continuous microscopic observations with geotechnical parameters obtained from a penetration well acquired during a geotechnical survey in the city of Rome. Several studies demonstrated, in fact, that interpretation of micromorphological features of soil can be used to support the calibration of qualitative and semi-quantitative compositional and textural data with physical parameters (Aslan & Autin, 1996; Schleuß *et al.*, 1998; Vissac, 2005; Styllas,

2014; Stoops *et al.*, 2018; Prokof'eva *et al.*, 2020, 2021). This approach has important implications in the proper management and monitoring of metropolises built on alluvial plains. Floodplains of urban rivers are prone to soil and subsurface modifications indirectly related to riverine flood influences on groundwater table (Bozzano *et al.*, 2000, 2008), extensive soil compaction associated with structural degradation and loss of porosity, and pedogenic modification associated with soil sealing and contamination from anthropogenic sources (Jim, 1998; Adderley *et al.*, 2010; Nirei *et al.*, 2014; Prokof'eva *et al.*, 2001, 2020, 2021). Thus, integrating geotechnical and meso and micromorphological observation is important to properly evaluate the soil geomechanical properties and adequately assess geological influences on environmental and engineering hazards.

GEOLOGICAL AND STRATIGRAPHIC SETTING

The studied area is located within the Roman Basin (Conato *et al.*, 1980), a Plio-Pleistocene extensional basin which stretches north and south of the Tiber Delta for about 135 km and that is mainly filled with sediment provided by the Tiber River (Fig. 1). This basin developed from the Late Pliocene along the Latium margin in connection with the opening of the back-arc Tyrrhenian Sea Basin, in turn related to eastward migration and rollback of west-directed Apennine subduction (Malinverno & Ryan, 1986; Patacca *et al.*, 1990; Doglioni *et al.*, 2004; with references therein). The development of the Roman Basin was accompanied by a continuous regional uplift (Milli, 1997; Bordoni & Valensise, 1998; Giordano *et al.*, 2003; Mancini *et al.*, 2007) and by the intense volcanic activity of the Roman Magmatic Province since the Pleistocene (Locardi *et al.*, 1976; Fornaseri, 1985; De Rita *et al.*, 1993, 1995; Peccerillo, 2005). Thus, its stratigraphic framework records a complex interplay among tectonic uplift, volcanic activity and Quaternary glacio-eustatic fluctuations (Cavinato *et al.*, 1992; De Rita *et al.*, 1994, Milli, 1994, 1997; De Rita *et al.*, 2002; Giordano *et al.*, 2003; Mancini & Cavinato, 2005; Mancini *et al.*, 2013a; Milli *et al.*, 2008).

The Roman Basin fill is constituted by several continental to marine low-rank depositional sequences (*sensu* Mitchum & Wagoner, 1991; Catuneanu *et al.*, 2009, 2011) with a duration variable from 30 to 120 kyr, stacked to form two composite high-rank sequences named Monte Mario Sequence (MMS, Lower Pleistocene) and Ponte Galeria Sequence (PGS, late Lower Pleistocene–Holocene; Milli, 1997; Milli *et al.*, 2008, 2013, 2016; Fig. 2).

The analyzed deposits belong to the most recent low-rank sequence known in the literature as Tiber Depositional Sequence (TDS) or PG9 sequence (Bellotti *et al.*, 1994, 1995), which developed entirely during the highstand systems tract (HST) of the PGS (Milli *et al.*, 2013, 2016). In particular, the TDS developed during the last glacial–interglacial cycle of post-Tyrrhenian age (last 120 kyr) and constitutes a still evolving sequence where all of the systems tracts occur. The lower boundary of this sequence is an erosional surface (Fig. 3), carved into the underlying Pliocene−Pleistocene deposits. The thickness of TDS ranges for the most part from <1 to 40 m, reaching approximately 80 m along the axis of the incised valley (Fig. 4).

The recent elaborated three-dimensional geological model of the area (Maffucci *et al.*, 2022) shows several NNW–SSE high-angle normal faults, dipping to the south-west, associated with coeval north-east/south-west transverse system. Both of these fault systems are responsible for the volcanic activity of the Roman Comagmatic Province (see Acocella & Funiciello, 2006, with references therein) and probably controlled the Tiber River path and local deviations. Most of these faults cut the TDS basal unconformity and deform the lower part of the TDS itself, indicating tectonic activity during the last 20 kyr.

The studied core (Figs 5 and 6), has been drilled in the alluvial deposits filling the internal sector of the Tiber incised valley. Here the lowstand (LST), transgressive (TST) and highstand systems tracts (HST) are constituted by channelized and floodplain fluvial deposits that contain a succession of immature palaeosols. The LST deposits are locally preserved and constituted by sand and gravel forming tabular bodies, 6 to 10 m thick, which have been attributed to a braided channel belt. The TST deposits are well-preserved and characterized by two main architectural elements: (i) vertically stacked channel bodies interpreted as deposited by meandering rivers; and (ii) genetically related floodplain deposits constituted by soft grey-bluish mud often very rich in organic matter, freshwater gastropods and peat layers, and locally associated with overbank and crevasse splay sandy silt deposits (Figs 5 and 6). The HST show a depositional context similar to TST, but with a reduced

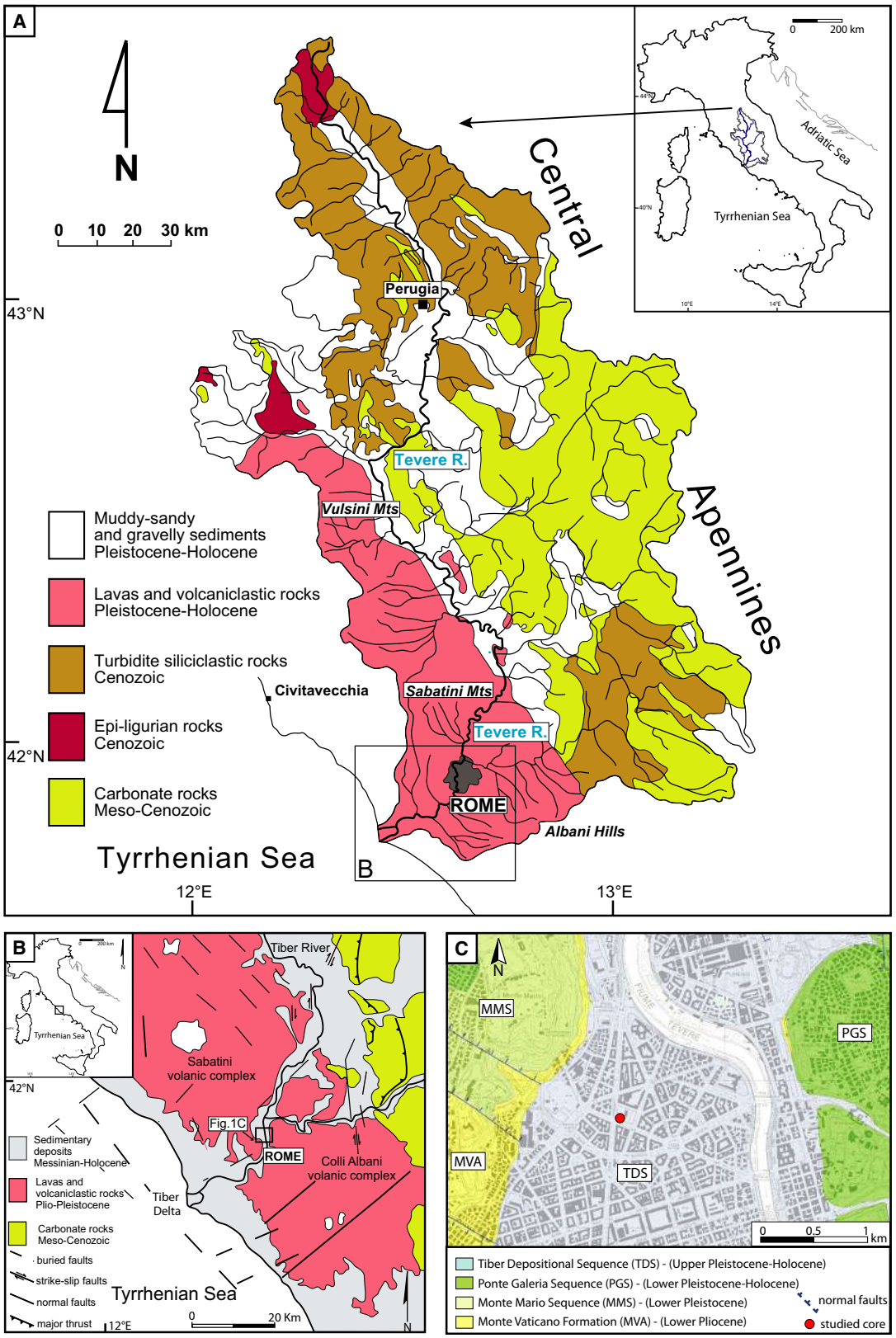

Fig. 1. (A) Tiber River drainage basin and main geologic units that crop out within the catchment. (B) Geological sketch of the central Tyrrhenian margin of Italy indicating the location of (C). (C) Stratigraphic map of the studied area in the Roman urban area (1 : 50 000) with studied core location.

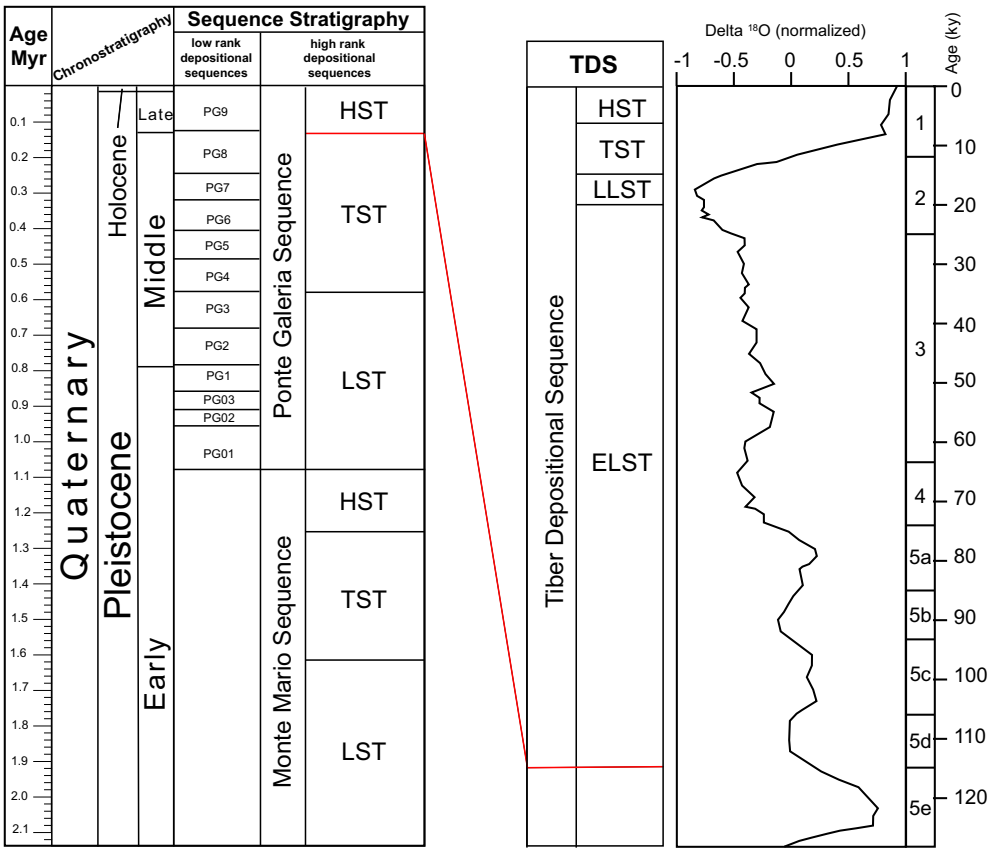

Fig. 2. Chronostratigraphic and sequence-stratigraphic scheme of the Roman Basin Quaternary deposits (modified after Milli *et al.*, 2016). HST, Highstand Systems Tract; TST, Transgressive Systems Tract; LST, Lowstand Systems Tract; ELST, Early Lowstand Systems Tract; LLST, Late Lowstand Systems Tract.

thickness of the deposits. Additionally, the fluvial-channel sand bodies tend to be wider than the underlying transgressive deposits and form a sandy amalgamated channel belt. Floodplain sediments are essentially represented by over-consolidated grey and brown mud with rare peat layers and with dry palaeosols, carbonate concretions and terrestrial gastropods (Milli *et al.*, 2013, 2016).

The composition of the studied succession reflects the source rock lithology of the Tiber drainage basin characterized, in the upper portion, by a Miocene turbidite succession and in the middle and lower portions by Mesozoic carbonates and Quaternary potassic and ultrapotassic volcaniclastic rocks of the Roman magmatic province (Fig. 1; see Tentori *et al.*, 2016, 2018).

METHODS

This work is based on a detailed facies and stratigraphic analysis of the Upper Pleistocene and Holocene alluvial deposits filling the Tiber incised valley occurring in the Rome urban area. Here, several coring boreholes, which provided lithological and textural information as well as qualitative and quantitative data on macro and microfauna content and radiocarbon age dates, were analyzed. These boreholes were used to construct some correlation panels showing the lateral and vertical stratigraphic relationships between the different lithological units (Figs 7 and 8). This was framed within the sequence stratigraphic scheme of the Tiber Upper Pleistocene to Holocene deposits proposed by Milli *et al.* (2016). Among the boreholes, one was selected for micromorphological, petrographic and geotechnical analysis. The analyzed continuously cored borehole (60 m deep) was chosen based on previous technical and sedimentological observations (Figs 5 and 6). The studied deposits are, in fact, representative of the main facies associations making up the majority of the alluvial subsurface in the city of Rome (see

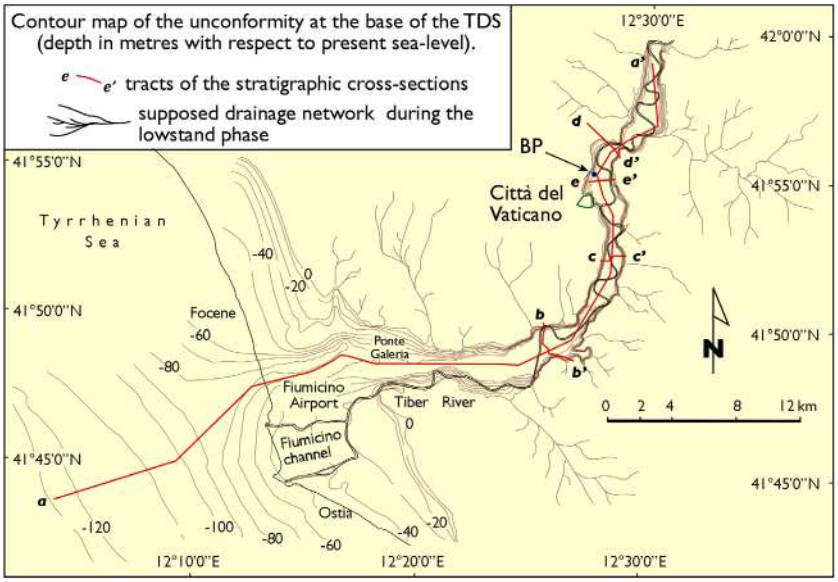

Fig. 3. Contour map (in metres) of the Tiber Depositional Sequence (TDS) boundary from Rome to the outer shelf. Red lines indicate the track of the stratigraphic cross-section reported in the paper. Black point indicates the location of the 'BP' borehole described in the paper (modified after Milli *et al.*, 2016).

Mancini *et al.*, 2013a, 2013b; Milli *et al.*, 2016; Di Salvo *et al.*, 2020).

Besides, in order to better constrain the stratigraphy and the compositional characters of the selected borehole, some of the surfaces of sequence-stratigraphic significance recognized in the coeval lagoonal and coastal deposits (see correlation panel of Fig. 4), were traced into the alluvial sediments; this allowed to evaluate the facies lateral changes among these depositional environments and to give a more relevant significance to the surfaces bounding the stratigraphic units individuated in the studied borehole.

Pocket penetrometer (PP), cone penetration tests (CPT) and Vs profile (Fig. 9) were acquired during a geotechnical survey in 2013 as part of a joint collaboration among CNR-IGAG, SAPIENZA University of Rome, and a private service company (Geoplanning S.r.l.). In addition to continuous visual examination of sediment texture and composition, micromorphological characterization of lithofacies and soil features were carried through petrographic, SEM and semi-quantitative XRD analyses. A total of 26 undisturbed samples were collected with an Osterberg sampler at different intervals to cover the whole spectrum of sedimentary facies. Thin sections of the coarser grain sizes (fluvial sand and overbank sand and silt deposits) were point-counted to investigate compositional characters and sediment provenance. Quantitative sand composition was defined using the Gazzi-Dickinson method (Ingersoll *et al.*, 1984) and counted grains grouped into monomineralic and polymineralic categories (Table S1). Recalculated parameters were plotted on QFL, QMKF and LmLvLs ternary diagrams to investigate sediment provenance by comparing our results with compositional data reported in Tentori *et al.* (2016, 2018), that describe the petrographic and compositional characters of the continental and marine deposits of the high-rank PGS sequence. Thin sections of organic-rich clay and silty clay deposits allowed to optically describe the main detrital and authigenic components, sediment texture and accessory material (fossils, plants and wood fragments). Micromorphological and semi-quantitative chemical analyses were performed on impregnated slices of clay and silty clay samples by SEM using a FEI-Quanta 400 (SEM-EDS; FEI Company, Hillsboro, OR, USA) instrument, operating at 20 kV, equipped with X-ray energy-dispersive spectroscopy at the Dipartimento di Scienze della Terra SAPIENZA Università di Roma. The SEM imaging was collected both in the secondary electron (SE) and back-scattered electron (BSE) modes. Energy-dispersive X-ray spectroscopy (EDS) spectra and X-ray maps were also acquired to highlight the elemental distribution through the sample. The EDS spectroscopy was used for elemental analysis and chemical characterization of major components. In order to evaluate bulk mineralogy, XRD analysis was directly performed on sample powder, using a Bruker D8 FOCUS diffractometer (Bruker Corporation, Billerica,

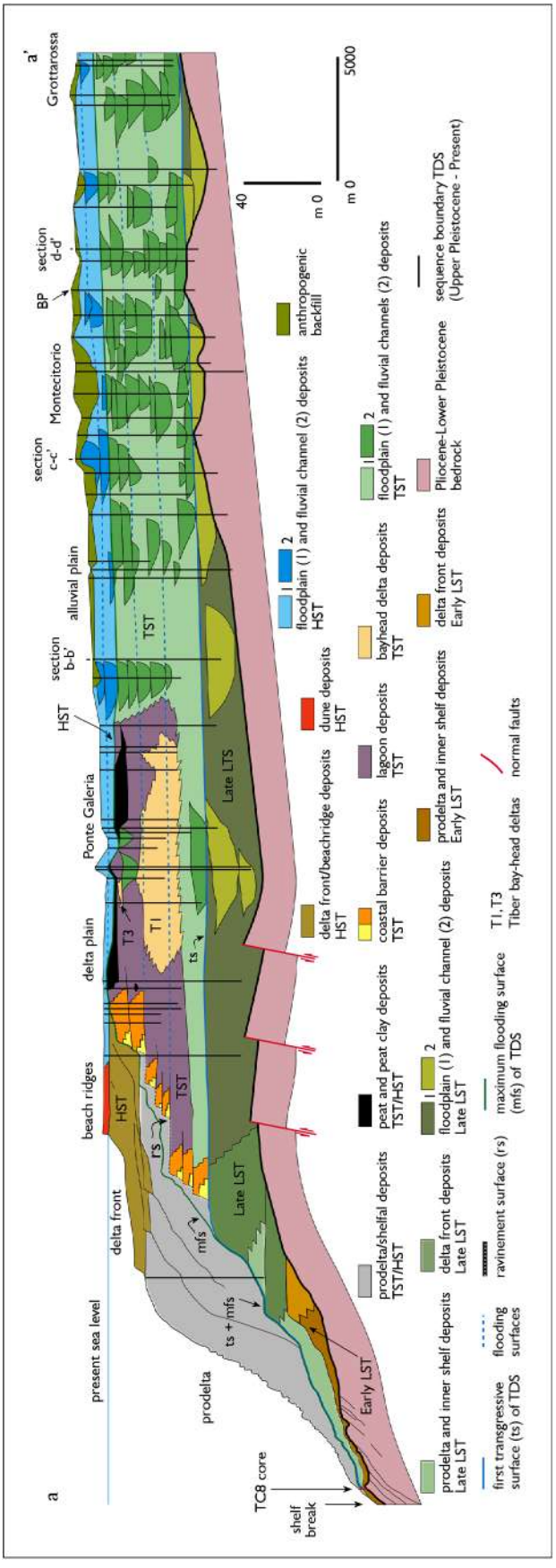

Fig. 4. Stratigraphic cross-section a–a′ (dip-oriented) showing the depositional architecture of the Tiber Depositional Sequence (TDS) and the location of the studied core (Bau Park core). For the track of cross-section, see Fig. 3 (modified after Milli *et al.*, 2016).

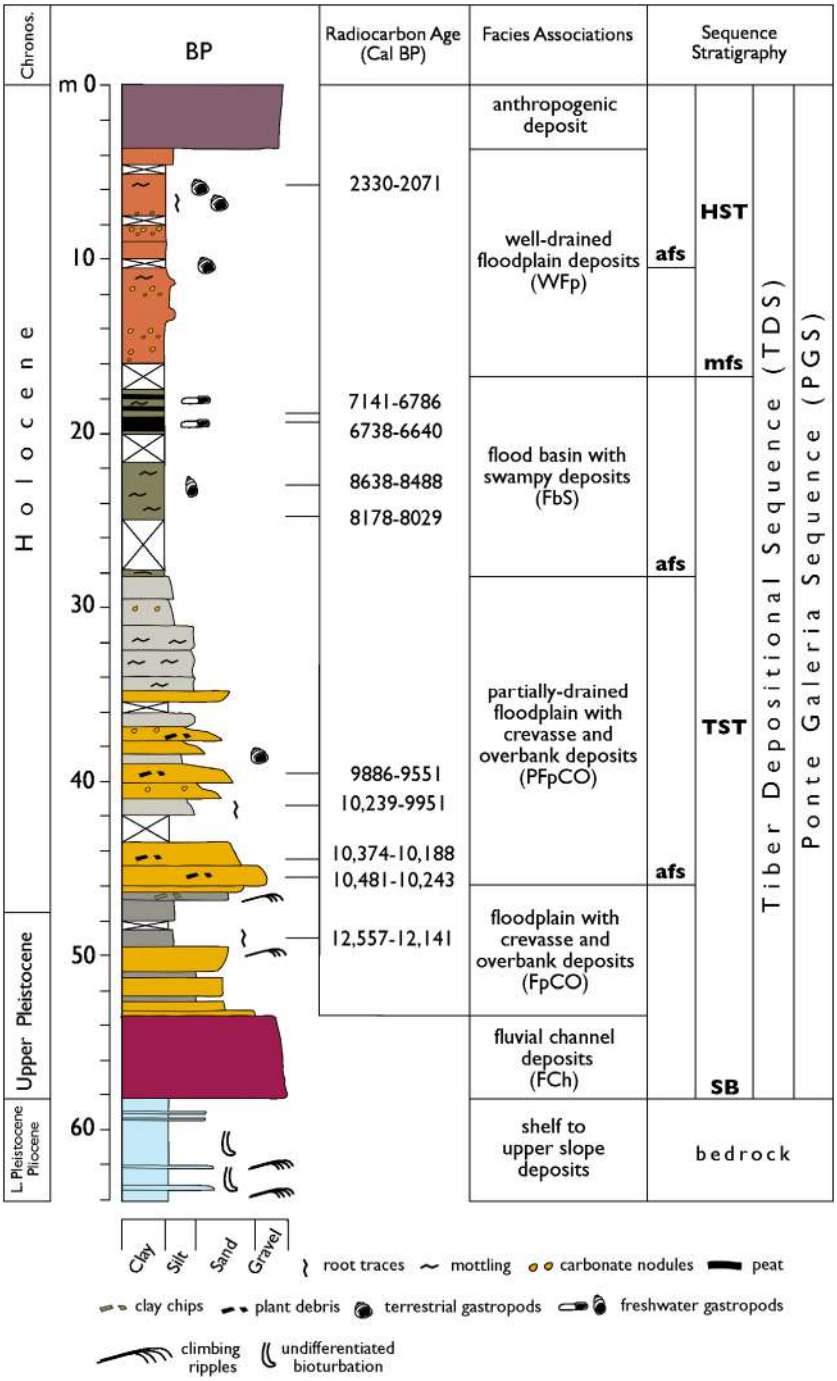

Fig. 5. Stratigraphic column of the 'BP' core showing the main facies associations, the inferred depositional environments and the sequence-stratigraphic interpretation. HST, Highstand Systems Tract; TST, Transgressive Systems Tract; SB, sequence boundary; mfs, maximum flooding surface; afs: alluvial flooding surface. Note in this case that the sequence boundary of the low rank Tiber Depositional Sequence (TDS) and the high rank Ponte Galeria Sequence (PGS) coincide. For the core location, see Figs 3 and 4.

MA, USA), with Cu Kα radiation on a Bragg-Brentano θ/2θ geometry, equipped with a Si(Li) solid-state detector, Sol-X (XRD Laboratory, IGAG-CNR, Montelibretti, Rome). Acquisition conditions were 40 kV and 40 mA. Scans were obtained from 20° to 80° 2θ with a count time of 2 s. The XRD data were processed using X-powder software combined with PDF2.DAT database of ICCD.

Description of facies associations by core analysis and interpretation of piezocone tests as well as a detailed microscopic investigation of organic, detrital and authigenic material is presented in the following sections. Textural classification of bulk sediment based on visual estimation of grain-size distribution is after Blott & Pye (2012), whereas terminology for descriptions of features seen in soil follows guidelines from Stoops (2021).

Fig. 6. Photographs showing the stratigraphy of the 'BP' core with the different facies associations and their environmental interpretation. Red line marks the sequence boundary separating the Tiber Depositional Sequence (TDS) from the underlying Lower Pliocene clay shelfal deposits of the Monte Vaticano Formation (MVF). First transgressive surface and sequence boundary coincide. The green line corresponds to the maximum flooding surface. The yellow line marks the position of the Paludification Surface (PaS). The white lines represent the boundaries between each facies association. Within the well-drained floodplain deposits note the local A/Bk horizonation.

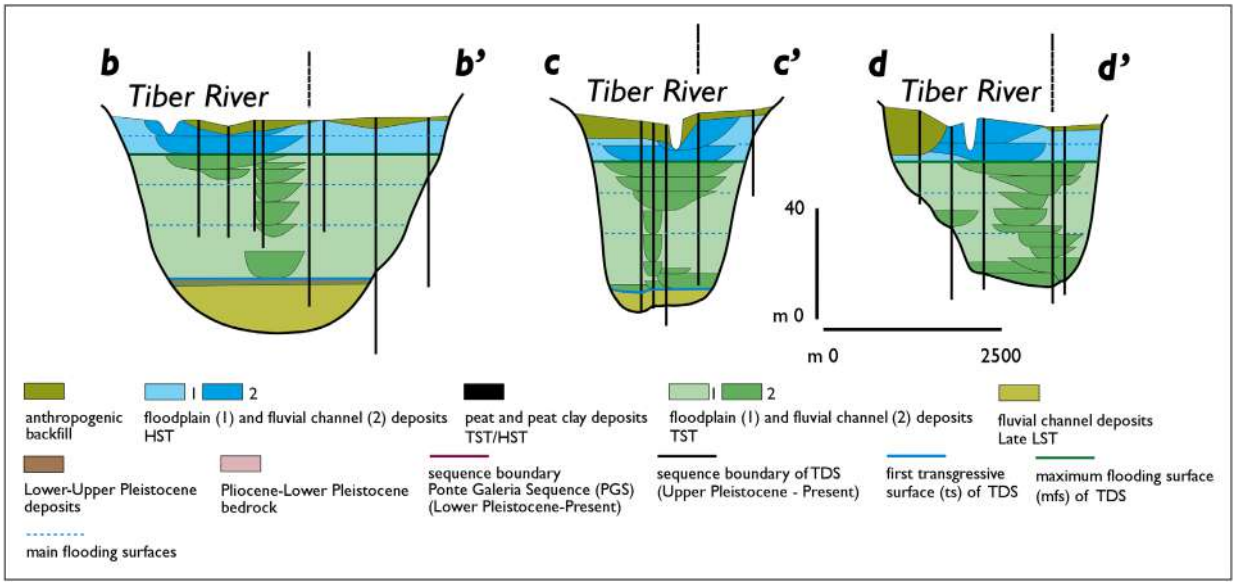

Fig. 7. Stratigraphic cross-sections showing the depositional architecture of the alluvial deposits within the Tiber valley. For the track of cross-sections see Fig. 3.

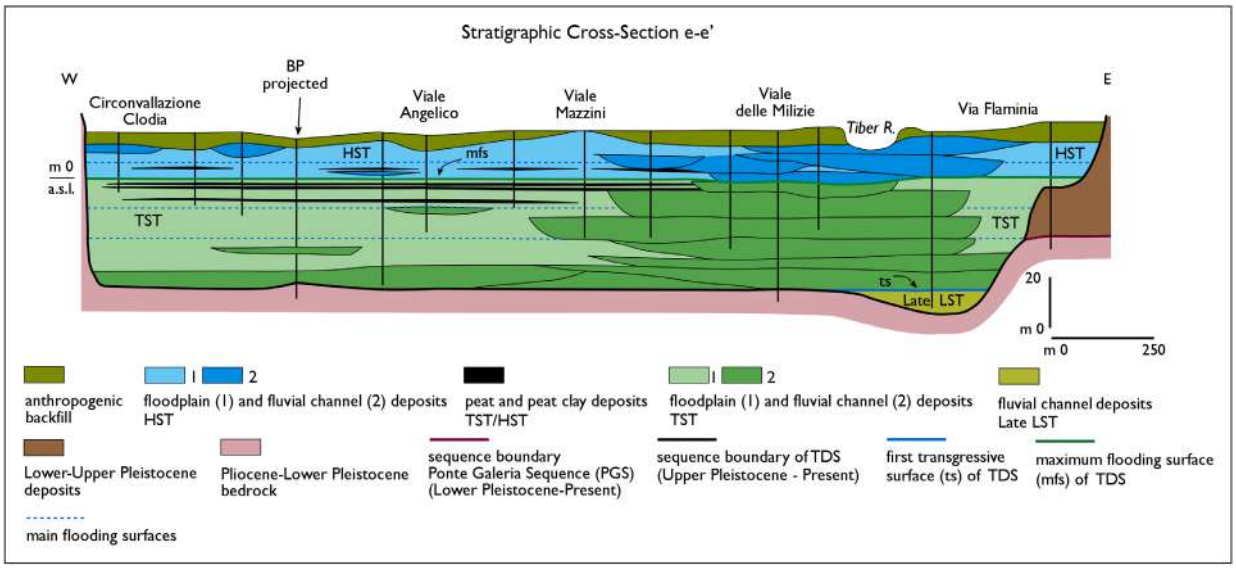

Fig. 8. Stratigraphic cross-section showing the depositional architecture of the alluvial deposits within the Tiber valley. For the track of cross-section see Fig. 3.

RESULTS AND DISCUSSION

Facies associations and sedimentological interpretation of piezocone tests

Five facies associations were identified in the deposits of the analyzed borehole and compared with the stratigraphy and sedimentological interpretation of the boreholes reported in Mancini *et al.* (2013b) and Milli *et al.* (2016). The CPTU interpretation is based upon three major parameters: corrected cone resistance (qc), sleeve friction (fs), friction ration (FR = fs/qc) and pore water pressure (u). These five facies associations

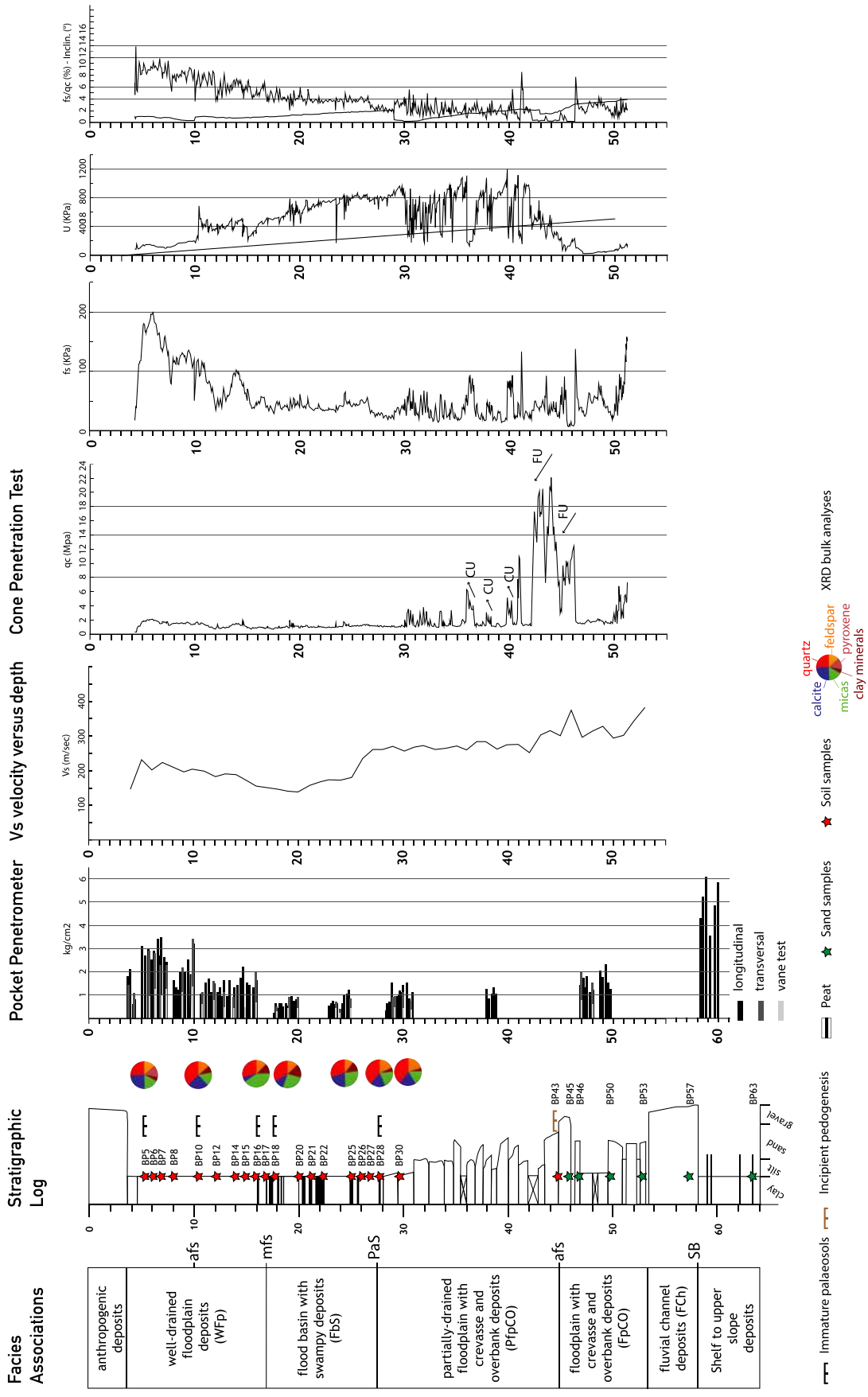

Fig. 9. Stratigraphic log of the 'BP' core showing the position of the samples used for micromorphological and compositional analyses, the identified palaeosols, and the X-ray diffraction (XRD) analyses (pie charts) of main mineral phases (quartz, feldspar, calcite, micas and clay minerals). On the right the main physical and geotechnical parameters of the studied deposits: pocket penetration (PP) values, Vs waves velocity profile versus depth, and piezocone penetration tests (CPTU). Vs velocity, pocket penetration values and CPTU parameters (qc—cone resistance, fs—sleeve friction and u—pore pressure) can be correlated with grain-size distribution and post-depositional textural modifications owing to pedogenesis (see text for details). Note that fluvial channel sands are characterized by fining-upward (FU) trends while overbank deposits are characterized by coarsening-upward (CU) trends.

include: (i) fluvial-channel deposits (FCh); (ii) floodplain with crevasse and overbank deposits (FpCO); (iii) partially drained floodplain with crevasse and overbank deposits (PFpCO); (iv) flood basin with swampy deposits (FbS); and (v) well-drained floodplain deposits (WFp) (Figs 5 and 9).

Fluvial-channel deposits (FCh)

Description. This facies association is characterized by grain size ranging from gravel to sand and mud, organized in fining-upward facies sequences, 3 to 5 m thick, with a sharp lower boundary and a sharp or transitional upper contact with the overlying muds (Figs 5 and 6). Gravels (1 to 5 cm in diameter) are essentially represented by well-rounded heterometric carbonate and chert fragments with subordinate sandstone clasts and rare volcaniclastic material (pumice and tuff). Sedimentary structures include low to high angle cross-stratification attributable to bedforms. Sand bodies show a diagnostic CPTU signature, with cone tip resistance values (qc) up to 22 Mpa, and decreasing upward, pore pressure (U) ranging from 100 to 800 Kpa and a low friction ratio (FR < 2; Fig. 9).

Interpretation. The comparison between these deposits and the surrounding ones, allows to interpret them as channel fillings attributable to braided channel belt (Figs 7 and 8). These channels form tabular bodies, 6 to 10 m thick, and internally show bedforms interpretable as dune and/or unit bar (terminology from Bridge & Demicco, 2008). Channels pass laterally to silty, sandy and muddy sediments interpretable as floodplain deposits. Upward these deposits are replaced by floodplain silty mud sediments; this fining-upward trend is also recognizable in the CPTU tests (Fig. 9). According to Milli *et al.* (2016), the erosional contact (see Figs 4, 7 and 8) between these fluvial deposits and the underlying Pliocene clay and silty clay shelfal deposits constitutes the sequence boundary of the TDS. Indeed, these channelized fluvial deposits occur at the base of the investigated succession and have been attributed by the previous authors to the initial portion of the transgressive systems tracts of the TDS.

Floodplain with crevasse and overbank deposits (FpCO)

Description. This facies association consists of rhythmically bedded sands, silty sands, silts and clayey silts, a few decimetres up to a metre thick, generally organized to constitute units with fining-upward and coarsening-upward trends (Fig. 5). The single units are generally packed inside thick portions of soft clay and mud containing freshwater gastropods. The centimetric silty sand and silt layers, internally show a climbing ripple cross-lamination and locally the presence of rootlets, whereas the thicker fine-medium sand beds (about 1 m thick) show a sharp base and a fining or coarsening-upward trend. No fauna has been recognized within this facies association that, locally, is overlain by fluvial channel (FCh) sands. The finer fractions (clay and silty clay) have low cone tip resistance values ($1.8 < qc < 2$), and pore pressure $U >> U_0$ (up to 1200 KPa). The sandy silt layers, which commonly display sharp bases, are characterized by qc values between 3 and 11 MPa, and pore pressure $U < U_0$. The overall FR of the deposits ranges between 1.0 and 8.0 (Fig. 9).

Interpretation. The characters of this facies association and its stratigraphic relationships with the lateral channelized deposits (see Figs 7 and 8) allow to interpret these sediments as the product of deposition in a floodplain environment where overbank and crevasse processes occurred. The silty sand layers with climbing ripples suggest deposition under decelerating sheet flows related to flood events whose velocity decreases away from the channel belt, whereas the muddy sediments record suspension fallout at the end of the flood events. The thicker sand beds are interpreted as crevasse splay or crevasse channels based on their lower sharp or erosive boundary. These facies associations can be distinguished from FCh bodies by the generally finer grain sizes and smaller thickness, a feature well-evidenced by the generally lower cone tip resistance (qc) and higher FR values (Fig. 9). The comparatively wide range of FR and U values indicates a wide spectrum of textures, local changes in grain sizes, reflecting repeated deposition of fine-grained detrital material transported by flood events in the floodplain area adjacent to the river channel.

Partially drained floodplain with crevasse and overbank deposits (PFpCO)

Description. This facies association is composed of varicoloured sand and silty sand beds forming a succession about 10 m thick bounded by light grey clay deposits containing rare carbonate nodules (Fig. 5). The latter occur, together with plant debris, rootlets and terrestrial gastropoda within the sand and silty sandy beds that are organized to form metre thick fining-upward and

coarsening-upward sequences (FU and CU, respectively). Compressive strength values derived from PP tests in the sand and silty sand beds range from 1.1 to 1.5 kg cm^{-2}. Cone tip resistance values (qc) from CPTU tests are between 1.9 to 22.0 MPa, and where these beds form CU sequences these resistance values vary, from bottom to top, from 2 to 3, 5, 6 and 11 Mpa. Pore-water pressure values are $<U_0$. The FR ranges from 1.1 to 8.0 (Fig. 9).

Interpretation. The FU and CU sand and silty sand units having plant debris, carbonate nodules and rootlets suggest deposition in a floodplain with overbank/crevasse sedimentation affected by incipient and local pedogenetic processes. These deposits accumulated in a more depressed sector of the floodplain due to more frequent flood events and were finally capped by muddy deposits when the flood events ceased. The values of compressive strength and cone tip resistance recorded by PP and CPTU are characteristic of partially to well-drained floodplain sediments (see also Amorosi & Marchi, 1999; Sarti *et al.*, 2012). In particular peaks in fs, U and FR (fs/qc%) (Fig. 9) are interpreted to represent the CPTU response to slight induration due to fluctuating groundwater levels and incipient pedogenesis.

Flood basin with swampy deposits (FbS)
Description. This facies association is constituted by unlaminated soft grey-bluish silty clay, very rich in organic matter and freshwater gastropods, and by peat layers (Fig. 5). The latter are less 1 m thick and are composed of wood fragments and other plant remains; they also contain a rich malacofauna of freshwater gastropoda. The CPTU tests indicate qc values constrained between 1.5 and 2 MPa with subtle peaks in qc and fs in correspondence with pore pressure (U) drops, the latter increasing for the most part linearly with depth (Fig. 9). Compressive strength (PP) values range between 0.5 and 1.2 kg cm^{-2}.

Interpretation. The soft silty clay deposits showing homogeneous colour, high content of organic matter, and the presence of freshwater gastropoda suggest deposition in a swampy environment developed in a shallow and subaqueous flood basin. The presence of peat layers and of deposits rich in organic matter confirm such an interpretation, which is also confirmed by the CPTU and PP values that are coherent with this interpretation. Where the development of peaty soils occurs, such deposits can be classified as Histosols (Soil Survey Staff, 2014).

Well-drained floodplain deposits (WFp)
Description. These deposits are composed of over-consolidated, grey to greenish and pale brown clay, mud and silt (Fig. 5). In these deposits, peaty layers are rare, while well-drained pedogenized-clayey levels are frequent. The latter are rich in rootlets, terrestrial gastropods (including *Cepaea nemoralis and Vallonia* spp.), carbonate concretions and light grey mottles. These deposits are characterized by a subtle increase in cone resistance (qc) with depth and a sharp fs (CPTU) and compressive strength (PP) peaks with the highest sleeve friction (fs) and friction ratio (FR) in correspondence with the uppermost section above the groundwater table and just below the anthropogenic layer (Fig. 9).

Interpretation. The sedimentological characters of these deposits allow to interpret them as the product of sedimentation in a well-drained floodplain affected by incipient pedogenetic processes. Where pedogenesis is more evident, these immature soils are typified by a darker organic-rich horizon (A) that overlies a paler calcic horizon (Bk; Fig. 6), and can be classified as Entisols according to Soil Survey Staff (2014). Palaeosols lying below the anthropogenic layer and down to 10 m depth, identified by the highest values of fs and compressive strength (PP) peaks, suggest slightly different conditions of soil formation or additional modification after burial (Fig. 9).

Petrography and soil micromorphology

Detrital grain composition and provenance of fluvial channel (FCh) and floodplain with crevasse and overbank (FpCO) deposits
Description. Sand collected from FCh (samples BP45 and BP57) and FpCO deposits (samples BP43, BP46, BP50 and BP53; Fig. 9) shows an overall homogenous composition and consists of abundant monomineralic quartz, common feldspar (K-feldspar and plagioclase) grains, and minor pyroxenes, micas (biotite and muscovite), iron oxides, and intrabasinal and extrabasinal bioclasts (Fig. 10A to H, J and Table S2). Rock fragments include abundant carbonate lithic with micritic and sparitic texture, common volcanic detritus with vitric, felsitic and microlithic textures, and minor low-grade metamorphic and siliciclastic lithic fragments. These main

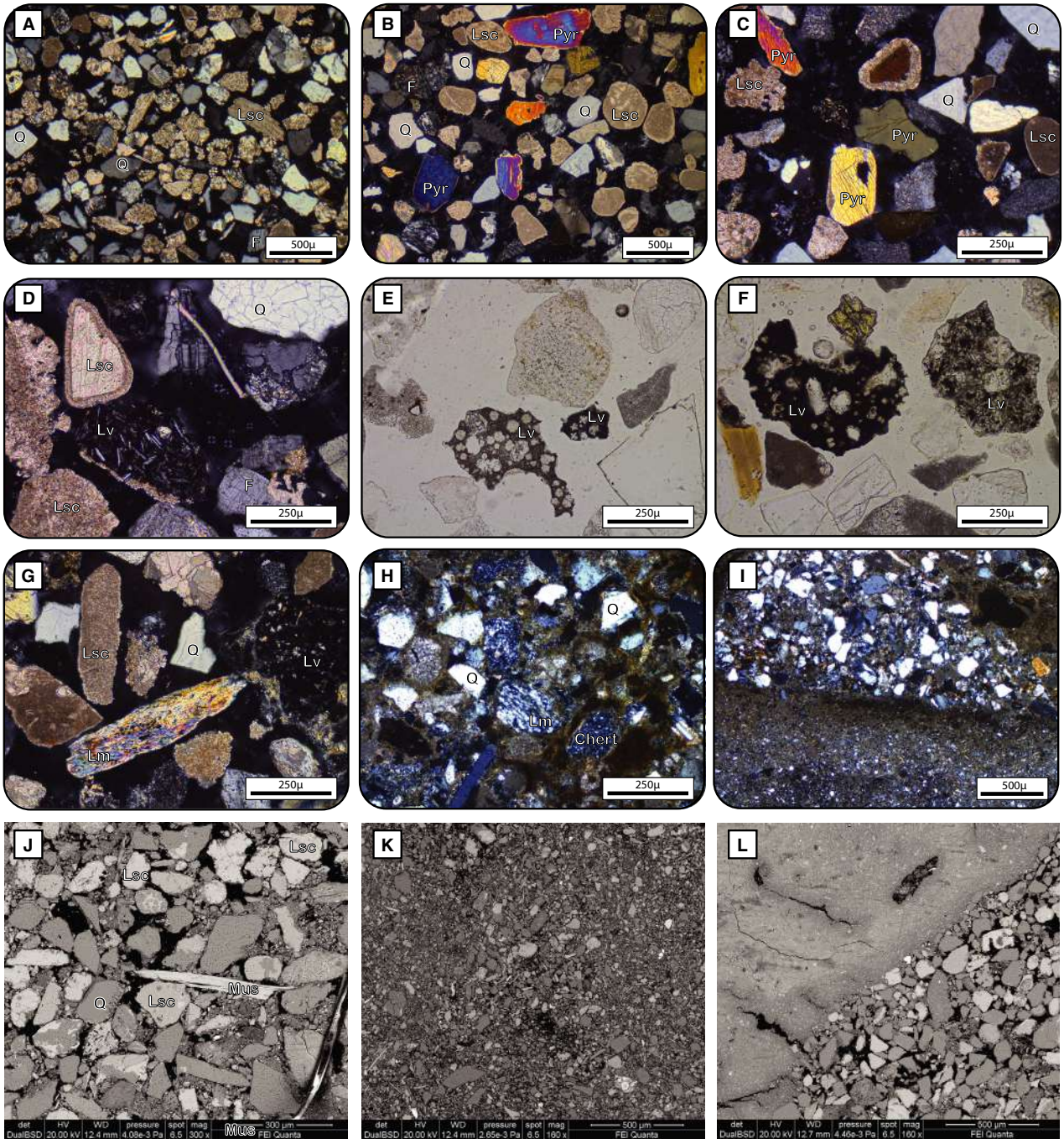

Fig. 10. Thin section views with main grain types from the Monte Vaticano Formation (MVA) and Tiber Depositional Sequence deposits (TDS). (A) MVA carbonaticlastic shelfal sand [Q = quartz; F = feldspar; Lsc = carbonate lithic fragment (crossed polars view or XPL)]. (B) to (F) TDS fluvial and overbank volcaniclastic sand with common volcanic lithic fragments (Lv) and pyroxene (Pyr) phenocrysts phases (XPL). (D) to (F) Fluvial and overbank volcaniclastic sand showing volcanic lithic fragments with microlithic texture (plane light view or PPL). (G) Metapelite lithic fragment (Lm) in overbank sand (XPL). (H) and (I) Sand and silt grain types from overbank deposits and infilling features related to depositional processes from floodplain facies associations (Chert = chert lithic fragment) (XPL). (J) Sand and silt from overbank deposits. (K) Faintly bedded silt (bedding is vertical). (L) Detail of infilling feature showing a sharp contact between clay and silt (Mus = muscovite).

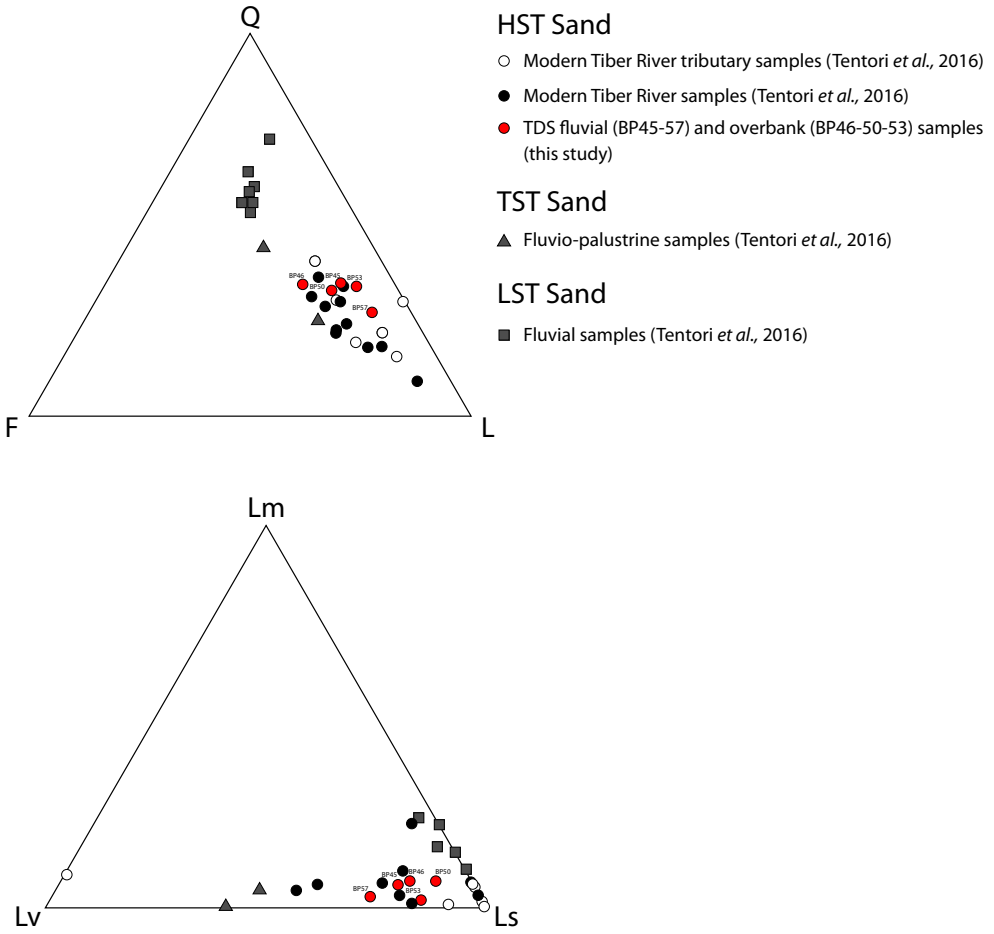

Fig. 11. QFL and LmLvLs ternary plots comparing the Tiber Depositional Sequence (TDS) alluvial deposits constituting the highstand systems tract (HST) of Ponte Galeria Sequence (PGS) with the transgressive systems tract (TST) and lowstand systems tract (LST) fluvial sand composition of the PGS. Note that TDS sand (this study) shows intermediate composition between Modern and Pleistocene sand (see also Tentori *et al.*, 2016).

components are the same as those recognized in detrital silt-sized samples from PFpCO, FbS and WFp deposits (Fig. 10I, K and L), which in addition exhibit common intrabasinal biogenic grains (terrestrial gastropods and undifferentiated carbonate shell fragments, siliceous diatoms, phosphatic and organic particles; see Fig. S1).

Interpretation. FCh and FpCO show compositional characters reflecting the proximal–distal relationship with respect to the channel location. This is well-evidenced in the distal floodplain overbank sand (samples BP46 and BP50; Table S2) that shows lower proportion of heavy minerals suggesting that denser grains are deposited in proximity to the main trunk river.

The sand composition of these two facies associations that were deposited during the HST of the higher rank Ponte Galeria Sequence (see Fig. 2), was compared with the PGS fluvial (LST) and fluvio-palustrine (TST) sand to investigate long-term temporal changes in sediment provenance (Fig. 11). Their comparison indicates that the HST deposits of the PGS ($Q_{33}F_{13}L_{54}$; $Lm_5Lv_{16}Ls_{79}$) overlap with the Tiber modern downstream sand from the main trunk and tributary streams ($Q_{28}F_{14}L_{58}$; $Lm_5Lv_{14}Ls_{81}$) on the QFL and LmLvLs compositional diagrams (Fig. 11), reflecting reworking of carbonate and siliciclastic units of the central Apennines and volcanic rocks of the Roman Magmatic Province (Fig. 1). Conversely, FCh and FpCO sand show intermediate LmLvLs composition between pre-volcanic LST ($Q_{61}F_{19}L_{20}$; $Lm_{15}Lv_1Ls_{84}$) and syn-volcanic TST sand ($Q_{35}F_{24}L_{41}$; $Lm_3Lv_{67}Ls_{30}$) of the PGS (Fig. 11). Sedimentaclastic and

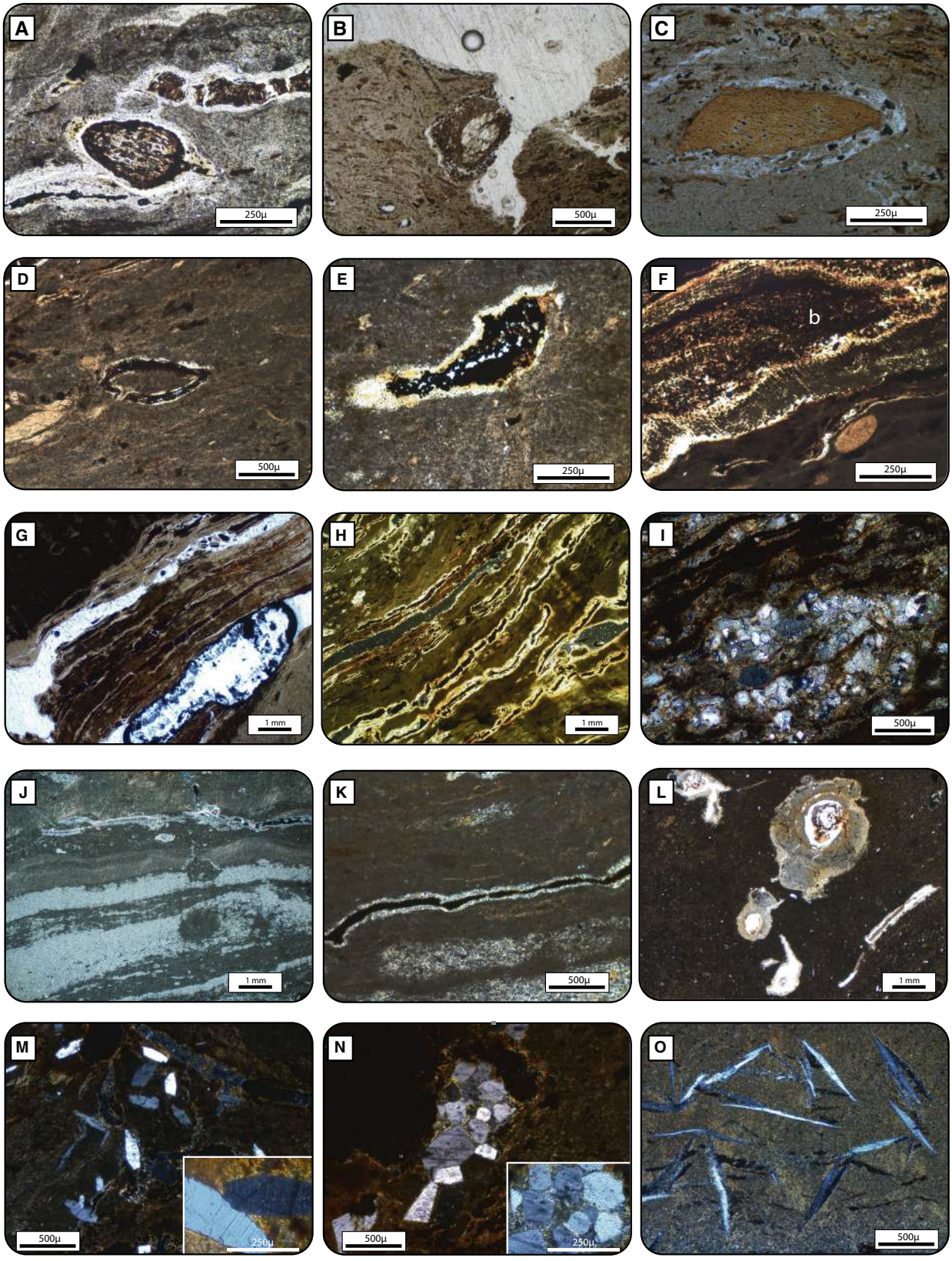

Fig. 12. Soil organic material and pedofeatures in flood basin and swampy facies association (thin section views). (A) Leaf in striated *b*-fabric showing minimal to no decomposition (planar view) (crossed polarized light, XPL). (B) Cross-section of needle leaf showing minimal to no decomposition (plane polarized light, PPL). (C) Possible seed remain showing minimal decomposition (XPL). (D) Decomposed leaf (plan view in XPL) in undifferentiated *b*-fabric. (E) Decomposed leaf in crystallitic *b*-fabric (section view in XPL). (F) Partially preserved bark remain (b) and organic phosphate grain (seed) (PPL). Note that these are more resistant to decomposition. (G) Multiple parallel lenses rich in decomposed organic material (PPL). (H) Wavy-organic stringers with birefringent hypo-coatings (XPL). (I) Infilling of calcite crystals (XPL). (J) Clay nodules within crystallitic *b*-fabric and bioclast rich interval with shell fragments and ostracods within organic clay (PPL). (K) Birefringent hypo-coating enclosing decomposed organic matter in striated *b*-fabric (XPL). (L) Roots encrusted with calcite (rhizoliths) (PPL). (M) Lenticular gypsum crystals and enlarged view (XPL). (N) Loose continuous void infilling with tabular gypsum crystals and enlarged view (bottom right) (XPL). (O) Acicular gypsum crystals (XPL).

quartzose LST fluvial sand suggests that before the beginning of volcanic activity, the palaeo-Tiber River was draining carbonate and siliciclastic sedimentary rocks of the central and northern Apennines. The sedimentaclastic signature was later diluted as the proportion of volcanic lithic content increased during deposition of the TST and HST of the PGS. In particular, the introduction of volcanic material is recorded by the syn-volcanic TST deposits which show the highest percentage of volcanic lithic fragments (see also Tentori *et al.*, 2016) whereas the HST post-volcanic lithic composition of the PGS was in part diluted by additional reworking of sedimentary source rocks from the lower course of the Tiber drainage basin. Alongside with release of volcanic detritus is the liberation of pyroxene phenocrysts that are concentrated by grain-density sorting in the FCh deposits (see Fig. 10B and C; Table S2).

Micromorphological features of flood basin and swampy (FbS) deposits

Description. Samples collected from FbS deposits (BP16, BP17, BP18, BP20, BP21, BP22, BP25, BP26 and B28; Fig. 9) are very slightly silty clay with abundant organic matter. The finer micromass shows a wide range of fabrics including undifferentiated *b*-fabric, calcitic and sericitic crystallitic *b*-fabric, and speckled striated and strial *b*-fabrics combined with abundant fine and amorphous organic matter. Pedofeatures include organo-sedimentary structures such as rhizocretions, roots casts, intact and decomposed leaves and plant remains, authigenic calcitic hypocoatings, and acicular, lenticular and tabular gypsum crystals occurring as single isolated crystals within the matrix and in aggregates around cracks and within cavities (Fig. 12). Organic-rich layers interbedded with poorly laminated silty clay consists of leaves (Fig. 12A to F) and wavy organic stringers, nodules, and aggregates (Figs 12G to I, K and 13A, G and H), and phosphatic particles (seeds and spores; Fig. 12C and F), diatoms and sponge spicules (Fig. S1). Cracks within organic stringers are locally filled with authigenic sparite cement (Figs 12I and 13J), and lenticular tabular, and acicular gypsum crystals (Fig. 12M to O). The BSE images and qualitative SEM-EDS elemental analyses (see Fig. S2) indicate the presence of pyrite occurring mainly as framboids both within the groundmass (Fig. 13D) and in association with plant remains (Fig. 13E, H and I), aggregates with radial arrangements of authigenic barite crystals (Fig. 13F), lenticular and acicular gypsum crystals (Fig. 13K) and heavy metals (for example, Cu, Ni and Cr) particles (Figs 13L and S2).

Interpretation. The main process occurring in the FbS deposits is the accumulation of peat, which means that organic matter is produced faster than it is decomposed (McCabe, 1985; Jerrett *et al.*, 2011). In this regard, different stages of plant decay can be observed: (i) an initial stage of decomposition characterized by discolouration of the plant tissue (Fig. 12A and B); (ii) an intermediate stage of decomposition with deformation of plant cell structure and shape (Fig. 12D and E); and (iii) a final stage with the formation of amorphous organic stain in the fine material (Fig. 12G, H and I; see also Stolt & Lindbo, 2010; Stoops, 2021). Associated with peat accumulation is the formation of minerals typical of reducing soils, such as pyrite (often in the form of framboids) and siderite (Fig 13C and D). Pyrite is by far the most common sulphide mineral occurring in these deposits. Associations between organic material and pyrite have been illustrated by several authors (Rabenhorst & Haering, 1989;

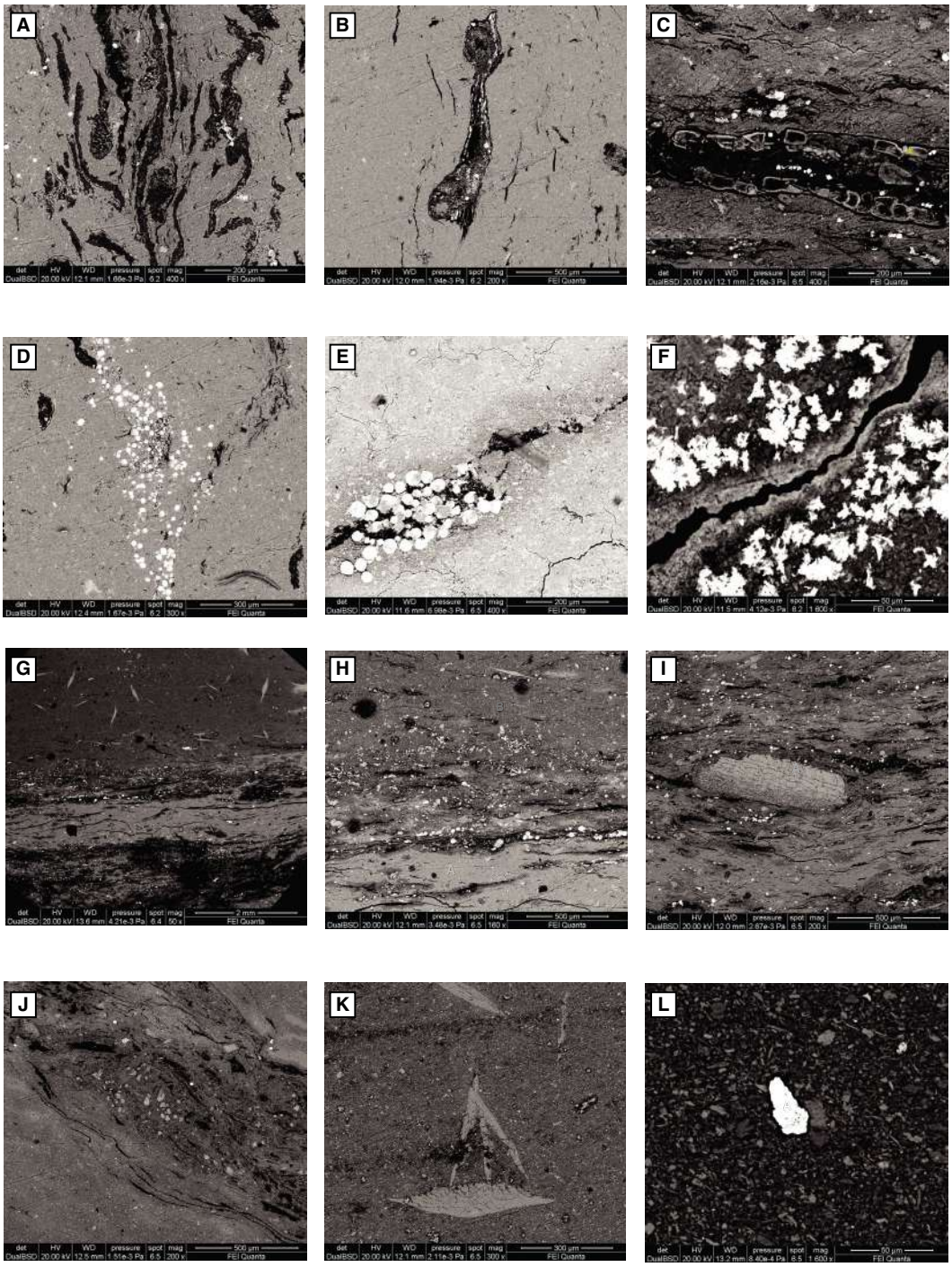

Fig. 13. Scanning electron microscope – back-scattered electron (SEM-BSE) images of soil pedofeatures in flood basin and swampy facies association. (A) Wavy organic residues (dark features) associated with aggregates of bright authigenic pyrite. (B) Organic matter (possibly leaf remain) with bright authigenic pyrite. (C) Calcium phosphate (yellow cross) revealed by energy-dispersive X-ray spectroscopy (EDS) analysis with 'ropy' texture (possibly replacing organic tissues as pseudomorphs plant tissue or spongy bone fragment) and bright pyrite within organic remain. (D) Pyrite framboids within the groundmass. (E) Clustered pyrite framboids associated with organic matter. (F) Barite crystals. (G) Organic-rich laminae (black features) with sulphates (bright spots) and gypsum crystals (arrows) within groundmass. (H) Same as (G) (enlarged view). Bright spots are authigenic sulphides (mostly pyrite). (I) Carbonate clast embedded within organic-rich clay. (J) Carbonate infillings (brighter grey) within organic stringers. (K) Acicular and lenticular gypsum crystals. (L) Copper particle.

Rabenhorst & James, 1992). Wada & Seisuwan (1986) suggested a relationship between degree of plant decomposition and pyrite formation, albeit our observations constitute an exception to this rule. Pyrite occurs in different stages of organic matter decomposition and its formation can be explained by taking in consideration several coexisting factors that include: (i) a source of iron (from iron oxides and iron compounds absorbed at the surface of clay minerals); (ii) the presence of sulphate ions from brackish water; (iii) the presence of sulphate-reducing bacteria within the groundmass and associated with organic material; and (iv) fluctuating reducing conditions.

The localized release of acids during organic matter degradation causes dissolution of calcareous materials (for example, carbonate rock fragments) that percolate from the soil solution into the matrix and precipitate in voids and cracks forming micritic hypo-coatings (Fig. 12K) and calcite infillings (Fig. 12I) (see also Sehgal & Stoops, 1972; Courty & Fedoroff, 1985; Kemp, 1995). In particular, the sparry calcite concentrated in voids is interpreted to be formed in groundwater (Figs 12I and 13J; see also Retallack, 2001). Other organo-sedimentary pedofeatures associated with calcification–decalcification processes result in the impregnation around decayed roots (for example, rhizocretions; Fig. 12L). Such pedogenic modifications may be due to desiccation processes during fluctuating dry conditions that result in the redistribution of carbonate, iron and phosphate within the soil matrix and precipitation of sparite cement, sulphides and sulphates minerals (for example, gypsum and barite). Another indication of high SO_4^{2-} concentration in combination with Ca^{2+} derived from the alteration of limestone rock fragments and carbonates of biological origin is the formation of gypsum. Gypsum occurs in acid sulphate soils (Poch *et al.*, 2018) and may form in the presence of organic matter. Lenticular and acicular gypsum crystals are associated with soil components that act as a source of sulphur or calcium, such as pyrite aggregates and shell fragments (Figs 12M, 12O and 13K) (Moormann & Eswaran, 1978; Charpentier *et al.*, 2001; Kostova & Zdravkov, 2007; Poch *et al.*, 2018). Clusters of roughly tabular gypsum crystals occur as infillings of voids and are related to fluctuations of the groundwater table (Fig. 12N; Yamnova & Pankova, 2013).

Precipitation of sulphates and sulphides could be also related to the landward migration of saline groundwater, testifying to the up-dip migration of brackish water within the incised valley (see also McCarthy & Plint, 1998). In such circumstances, the sulphate-rich waters penetrating peat layers, could have been used by sulphate reducing bacteria to produce H_2S, and reacting with Fe to form pyrite (FeS_2; see also Horne *et al.*, 1978; Holz *et al.*, 2002).

The SEM-EDS elemental analyses detect significant amounts of Cu, Ni, Cr at the base of the FbS facies associations (Figs 13L and S2). Heavy metals in these deposits should derive from the leaching of parent detritus and their concentration is affected by many factors inclusive of, but not limited to, pH, redox status and water contents. Metal transport in rivers and accumulation in floodplain soils is also determined by the movement of humus acids and their subsequent deposition (Alloway, 2012). Copper has the strongest affinity for humic and fulvic acids. Sulphides are a source of Cu, and soils containing high amounts of clay minerals and organic matter generally show relatively high concentrations of natural Cu (Oorts, 2012). Nickel is often associated with sedimentary rocks and is interpreted to derive from weathering of silicate minerals such as augite and biotite. Nickel has an affinity with soil organic matter and occurs in alluvial soils originating from volcanic source rocks (Gonnelli & Renella, 2012).

In summary, our observations suggest that deposition occurred for the most part in submerged and reducing environments. However, peaty horizons are associated with carbonate and clay-rich horizons containing carbonate concretions and suggest the existence of pedogenetic processes linked to water-table oscillations.

Micromorphological features of well-drained floodplain (WFp) deposits

Description. Samples collected from WFp deposits (BP5, BP6, BP7, BP8, BP10, BP12 and BP14; Fig. 9) vary from very slightly sandy silty clay to sandy silty clay. Thin sections dominated by silt and very fine sand grains, which are generally surrounded by clay coatings, show a porphyric fabric whereas the finer-grained samples groundmass is dominated by a mixture of clay and clay-sized carbonate (calcitic crystallitic and undifferentiated *b*-fabric). Pedofeatures include carbonate micritic nodules and mottles of irregular shape (Fig. 14A and B), rounded accumulation of illuviated clay (Fig. 14B and J),

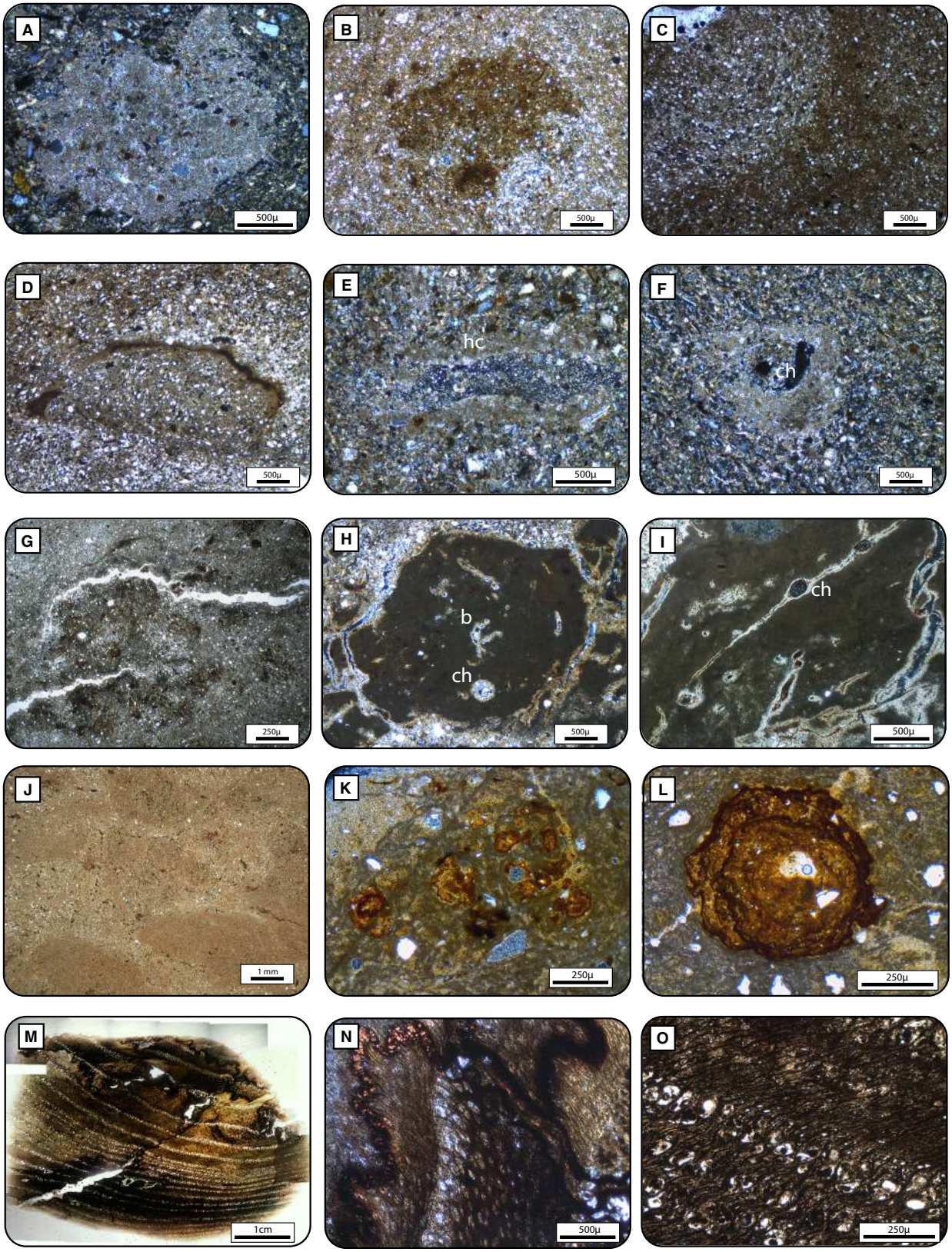

Fig. 14. Thin section views of soil pedofeatures in pedogenized and well-drained floodplain facies association. (A) Orthic carbonate micritic nodule. Note the presence of detrital grains in the nodule and its irregular boundaries pointing to an impregnation or substitution (crossed polarized light, XPL). (B) Clay mottle (XPL). (C) Cross-section through a channel infilling composed of silt grains and clay with a porphyric c/f-related distribution pattern. Void and infilling are related to faunal passage feature (plane polarized light, PPL). (D) micritic carbonate hypo-coating enclosing a root/plant residue PPL. (E) Channel surrounded by external calcite hypo-coating (hc) (XPL). (F) Calcite hypo-coating on channel (ch) (XPL). (G) Desiccation cracks (planes void) in clay-rich intervals within a calcitic crystallitic *b*-fabric (PPL). (H) Burrows (b) and root related channels (ch) with internal micritic coatings in undifferentiated *b*-fabrics (XPL). (I) root related channels (ch) in undifferentiated *b*-fabrics (XPL). (J) Rounded infiltrated clay, nodules and with plant remains (PPL). (K) Irregular iron nodules in fine calcitic crystallitic *b*-fabric (XPL). (L) Rounded Fe-nodule and scattered grains in fine calcitic crystallitic *b*-fabric (PPL). (M) Thin section views of charcoal fragments (PPL). (N) Lignified tissue (XPL). (O) Thick-walled cells (PPL).

calcite hypo-coatings (composed of micritic carbonates formed from soil solutions percolating along the soil fissure, Fig. 14E and F), Fe-nodules (Fig. 14K and L), as well as organo-sedimentary structures including rhizoliths, burrows, channel infillings (pedotubules filled with detrital grains, Fig. 14C), scattered plant remains (Fig. 14D) and lignite remains (Fig. 14M, N and O). The finer material shows a complex network of desiccation cracks, burrows, branching root traces and root-related channels filled with authigenic micrite and sericite (Fig. 14G, H and I). SEM-BSE and qualitative EDS elemental analysis (Fig. S2) indicates the presence of authigenic iron oxides (for example, hematite and ilmenite), sulphates (for example, barite), and carbonate cement within cracks (Fig. 15H to L).

Interpretation. Micromorphological evidence suggests incipient pedogenization under fluctuating drying and wetting conditions. Cracks are the result of physical processes related to desiccation whereas mottling is usually associated with alternation of oxidizing and reducing conditions within a zone of water-table fluctuation (Kraus & Aslan, 1993; McCarthy *et al.*, 1998). Dissolution and reprecipitation of calcite-saturated water with respect to calcite during water-table fluctuation or due to evaporation processes led to the formation of impregnative features, including calcite nodules and coatings around void walls and organic matter remains (see also Fedoroff *et al.*, 2010; Adderley *et al.*, 2018). In particular, hypo-coatings around channels and plant remains are composed of micritic and microsparitic carbonates formed from soil solutions percolating along the pores or fissures and penetrating into the soil matrix (Sehgal & Stoops, 1972; Courty & Fedoroff, 1985; Kemp, 1995) or after rapid precipitation of calcium carbonate due to root metabolism (Wieder & Yaalon, 1982). According to Klappa (1980), rhizoliths result from precipitation of carbonate around root channels and plant remains in dry and alkaline conditions following water table fluctuations and repeated cycles of wetting and drying. Under these conditions, roots margins alternately became wet and acidic (dissolving carbonate) and dry and alkaline (precipitating carbonate) and became progressively encrusted with calcite, preserving the hole as the root dies (see also Esteban & Klappa, 1983).

The presence of rounded soil Fe-concretions is related to processes of reduction, translocation and oxidation of Fe and Mn oxides during a seasonally fluctuating water table, and may be indicative of a perched water table developing above an indurated horizon acting as a natural barrier and restricting water infiltration (Gasparatos, 2012; Vepraskas *et al.*, 2012; Szymański & Skiba, 2013).

Loose infillings composed of silt and fine sand, result from deposition of fine material in open voids by surface and percolating water. Other types of infilling are interpreted as faunal voids filled with grains transported by soil animals such as termites (for example, passage feature; Kooistra & Pulleman, 2010; Marcelino *et al.*, 2018; Figs 14C and 15C). Clay illuviation and low preservation of organic matter suggest generally oxidizing conditions. In this context, the presence of sulphates (for example, barite), identified through SEM-EDS analyses, appears to be related to organic matter oxidation, saline groundwater and hydromorphic or slightly hydromorphic conditions (Chow & Goldberg, 1960; Stoops & Zavaleta, 1978; Bullock *et al.*, 1985). Barite precipitation may be an indicator for marine or brackish water incursions (Fig. 15H).

All of the described soil micromorphological features are characteristic of weakly developed (immature) palaeosols (for example, Entisols

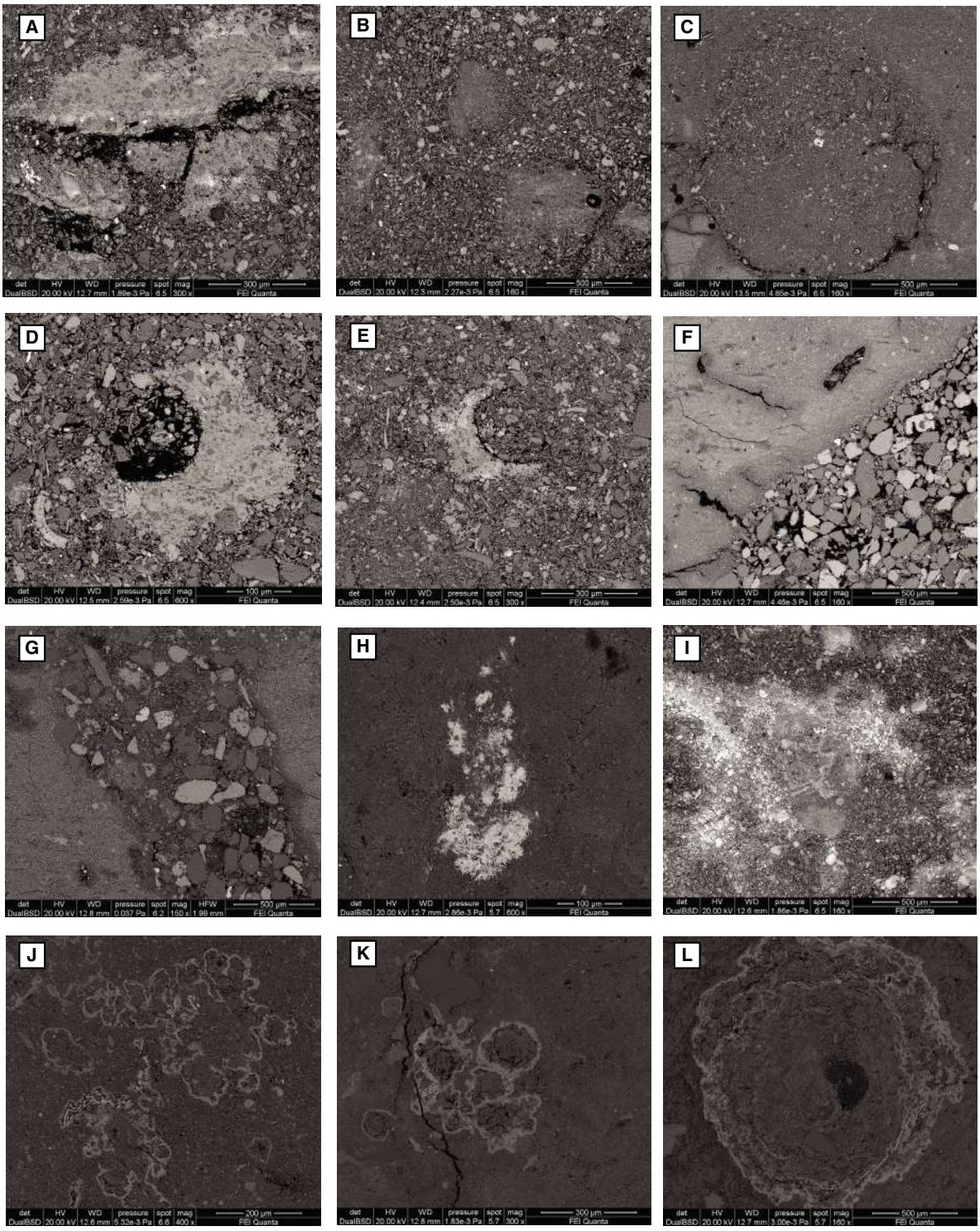

Fig. 15. Back-scattered electron (BSE) images of soil pedofeatures in well-drained floodplain facies association. (A) Calcite nodule (fractured) containing quartz and feldspar grains and iron oxides/Mn oxide inclusions. (B) Clay mottles. (C) Channel with infilling of illuviated clay and silt-sized grains of possible biological origin. (D) Calcite hypo-coating on channel (ch). (E) Calcium carbonate encrusting root (for example, rhizolith). (F) Sharp contact between sand and clay. Coarser grains are interpreted as loose infilling related to depositional processes. (G) Sand-sized channel infilling. (H) Barite crystals. (I) Ferruginous groundmass with irregular Fe-nodule. (J) Irregular composite Fe-concretions. (K) Composite Fe-concretions. (L) Rounded Fe-nodule.

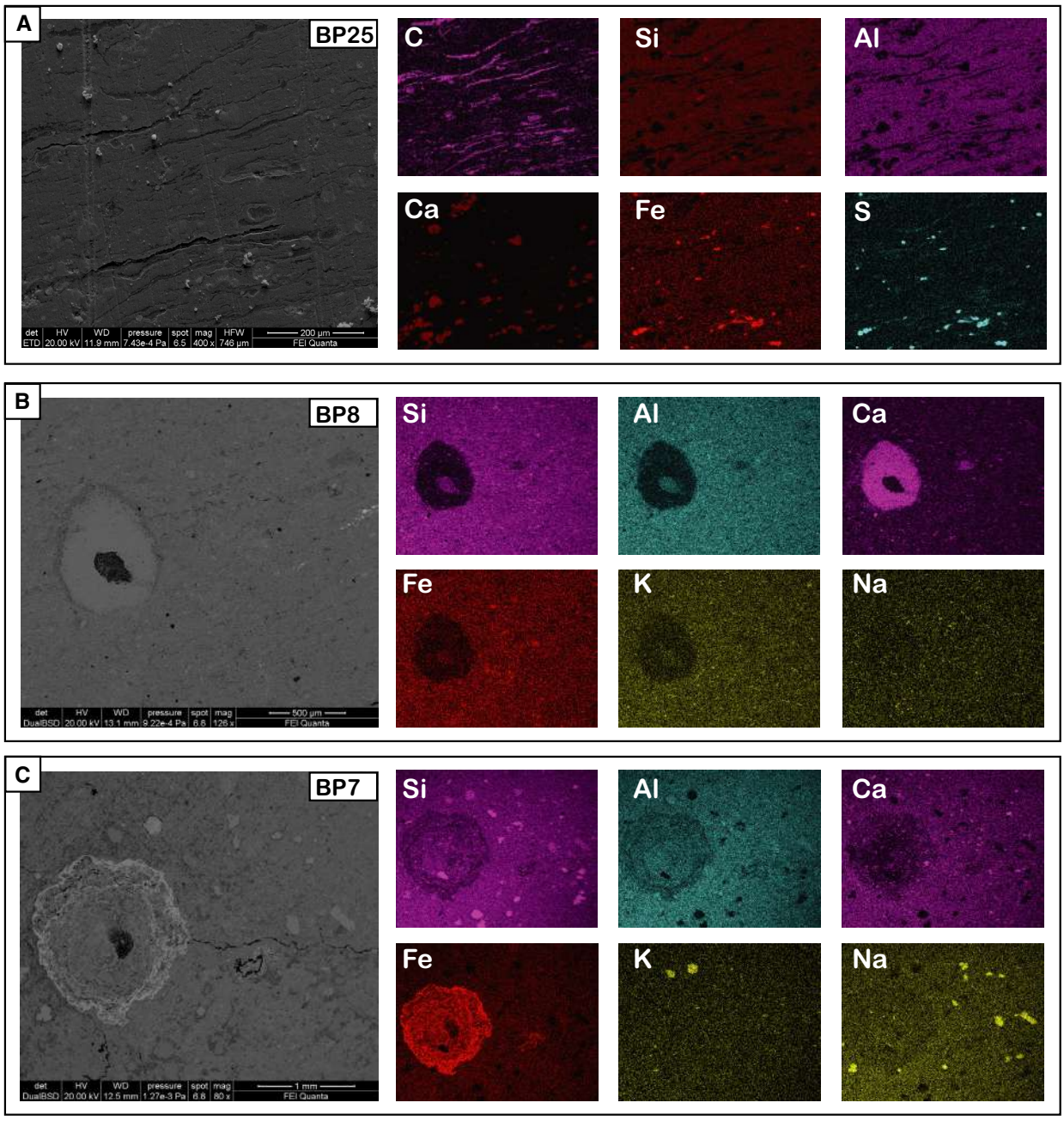

Fig. 16. Back-scattered electron (BSE) imaging and X-ray maps of samples BP7, BP8 and BP25, representative of pedogenized well-drained and peaty soil deposits, showing the compositional variation of Si, Al, Ca, Fe, K, Na, C and S. Note in sample BP25, the presence of Ca infilling, and organic stringers enriched in C and associated with Fe and S, forming pyrite framboids. BP8 shows Ca-hypocoating whereas in BP7 a Fe-rich nodule, and scattered quartz and feldspar grains were observed. Note also that the groundmass in BP7 and BP8 is enriched in Ca (see Fig. 14 for thin section view).

according to Soil Survey Staff, 2014), which mark short-lived phases of subaerial exposure (Retallack, 2001; Buol *et al.*, 2011) that are normally found on young geomorphological surfaces such as floodplains and alluvial sequences (Retallack, 2001).

Correlation between micromorphology and geotechnical data

Sedimentological observations integrated with the analysis of soil micromorphology and

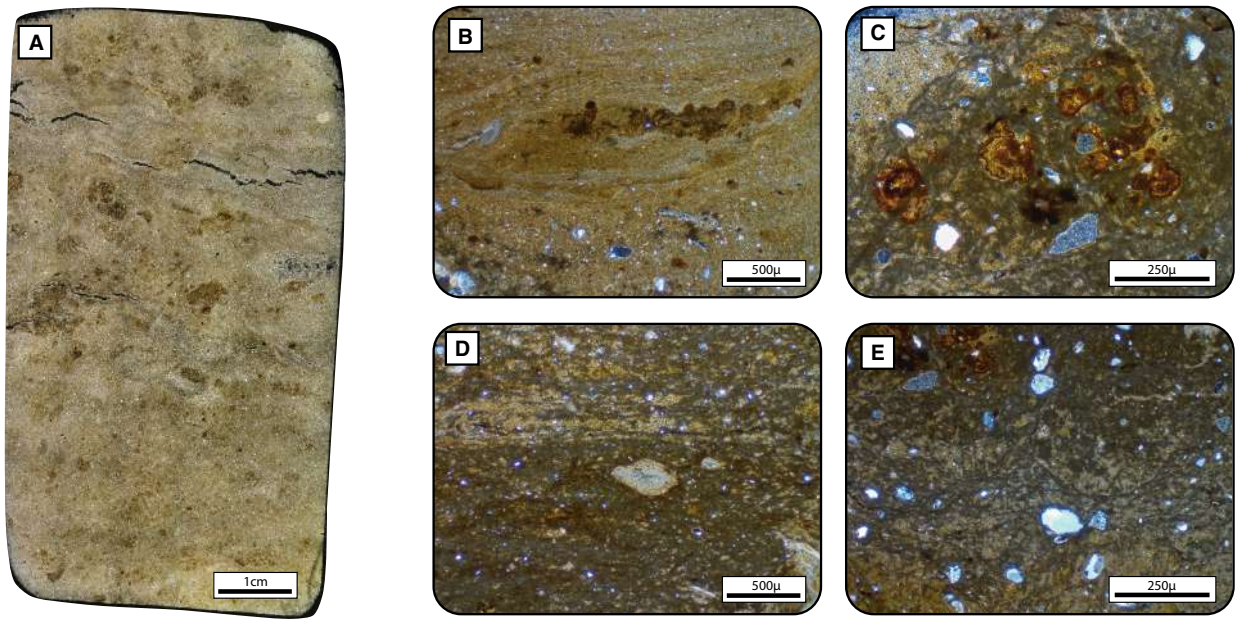

Fig. 17. Thin section views (A) to (E) of well-drained and pedogenically modified floodplain deposits showing a characteristic calcitic crystallitic *b*-fabric with clay nodules, carbonate concretions and scattered silty grains and Fe-nodules. Indurated carbonate-rich horizons from the upper core show the highest penetration values (see Fig. 9).

geotechnical data (Fig. 9) allow to investigate the factors and the sedimentary processes determining the physical properties of each facies association. In particular, CPTU measurements seem to be influenced by a number of interrelated factors including compressibility, grain-size distribution, mineralogy and grain shape (see also Cai *et al.*, 2014) and whose contribution can be better evaluated thanks to detailed textural, petrographic and micromorphological analyses.

Geotechnical properties of the FCh and floodplain with crevasse/overbank deposits are especially affected by the sediment grain-size distribution. This is well-illustrated by the characteristic channel infill showing a fining-upward trend recognizable in the cone tip resistance values of CPTU tests and can be also deduced by looking at the spectrum of qc and fs values within the overbank deposits, that record a heterogenous succession of contiguous sandy and silty layers (resulting from extensive channel crevassing during periodic flooding) alternated with floodplain clay. This study also observed a more general trend of upward decreasing particle size typified by decreasing cone tip resistance and sleeve friction values. Grain-size decrease in the floodplain is connected with a step-wise rising of the river depositional base level that determines a cyclic formation of depositional units in response to change in relative sea level.

The finer-grained floodplain facies associations (clay and silty clay) show more homogenous cone tip resistance values (qc) but variable fs and FR between FbS and WFp deposits. In the FbS facies associations, the most important feature influencing the geotechnical properties of clay is the presence of organic matter. Organic soils (with organic content greater than 20%) are associated with high plasticity, high shrinkage and high compressibility that contribute to its poor engineering characteristics (see also Mitchell & Kenichi, 2005; Kazemian, 2015; Ou & Fang, 2017). The CPTU tests indicate an overall uniform behaviour with subtle peaks in qc and fs that could be related to different degree of organic matter decomposition. Peaty horizons (with organic content exceeding 75%) can in fact be classified according to their fibre content and degree of humification or decomposition into fibric, hemic and sapric peat and show different behaviours in terms of compressibility, shear strength and permeability (Mitchell & Kenichi, 2005; Kazemian, 2015). Our micromorphological observations (Fig. 12A to H) document different stages of organic matter decomposition and seem to validate this hypothesis.

Besides organic-matter content, precipitation of secondary calcite can be considered another important discriminatory factor between the physical behaviours of FbS deposits, the latter showing the highest Ca amount at the top of the succession (see also XRD bulk analyses in pie charts of main mineral phases of Fig. 9). The degree of stiffness within pedogenically modified deposits appears to be related to induration processes that mark phases of subaerial exposure due to precipitation of secondary carbonates and iron oxides related to groundwater fluctuations within the soil horizon (Figs 16 and 17). Impregnative features, including calcite nodules and hypo-coatings are interpreted as being developed through dissolution and precipitation during evapotranspiration in alternating wet and dry conditions and related to leaching of calcareous detritus and subsequent precipitation from soil solutions into the soil matrix. This complex mix of detrital, pedogenic and groundwater carbonates is a common feature in surface soils in seasonally dry riverine plains (Stolt & Lindbo, 2010) and release an identifiable fingerprint into the CPT values.

A further process responsible for the extensive over-consolidation within the uppermost 10 m of the succession, is possibly the precipitation of additional fine-grained carbonate within the soil matrix (Fig. 17) associated with leaching from calcareous building debris derived from the above anthropogenic layer (for example, cement, mortar, concrete, brick fragments; Jim, 1998), which increases the area of grain contact (i.e. reduces porosity) and hardens the pore structure (Kenter *et al.*, 2007; Husseiny & Vanorio, 2015). In this regard, indurated compound soils may have acted as a dense natural barrier to water infiltration, leading to seasonal groundwater saturation and subsequent leaching of the above anthropogenic layer. Accumulation of calcium carbonate linked with soil contamination by construction debris has been observed in modern urban soils (for example, Moscow; Prokof'eva *et al.*, 2020) and is a frequent feature in many archeological sites (Adderley *et al.*, 2010; Itkin *et al.*, 2016). The common characteristics in urban soils are the redistribution of calcium carbonate within the micromass evidenced by the formation of calcitic crystallitic *b*-fabric and the authigenic precipitation of calcite coatings and infillings pedofeatures (Figs 14 and 17). Carbonate crystal size is commonly fine (micritic) because of rapid evaporation and/or transpiration leading to high levels of supersaturation and rapid precipitation but sparite cement also occurs. Alongside with increased fs and FR ratio parameters, micrite precipitation within the matrix results in a slight increase of the S-wave velocity given that the seismic properties (for example, P-wave and S-wave velocities) are largely controlled by the contacts between grains and porosity (Kenter *et al.*, 2007; Husseiny & Vanorio, 2015; Fig. 9). Analyses on Holocene uncemented soils, show, in fact that the qc or Vs values depend mostly on the void ratio (for example, density index), and effective stress and compressibility (Fear & Robertson, 1995; Cai *et al.*, 2014).

Understanding the intrinsic characteristics of urban soil, including textural and micromorphological features, has important implication to assess potential engineering hazards related to local seismic amplification and influenced by the anthropic layer contamination.

The depositional history and the stratigraphic context of the BP core

Micromorphological features along the studied core were framed within the depositional context and the sequence stratigraphic scheme from the TDS alluvial deposits, to characterize petrographic changes across major stratigraphic surfaces. In particular, compositional and textural features reflect major facies changes, the environmental conditions of soil formation, the cause–effect relationship between detrital and authigenic mineral composition and the coexistence of pedogenic and geological processes; these processes are the expression of the close interaction between change in accommodation space and sediment supply. The early development of the fluvial succession was characterized by river incision into the marine deposits of the Monte Vaticano Formation, followed by deposition and fluvial aggradation during the late lowstand, transgressive and highstand systems tracts of TDS (Figs 4, 7 and 8). Following the base level/sea-level fall responsible for the Tiber incised valley formation, a palaeodrainage rearrangement is recorded by the sharp facies changes and by a significant textural and compositional change across the TDS sequence boundary. The sandy transgressive fluvial deposits of the TDS, show a change in lithic fragment composition with respect to the older Plio-Pleistocene deposits, especially in terms of Ls to Lv proportion (from $Lm_5Lv_1Ls_{94}$ to $Lm_5Lv_{16}Ls_{79}$), and document the presence of volcanic material, introduced into the system through the extensive reworking of the Middle–

Upper Pleistocene volcaniclastic rocks of the Roman Magmatic Province cropping out into the Tiber drainage basin (Figs 10 and 11; Table S2).

In the Tiber incised valley the TST deposits of the TDS (Figs 7 and 8) show an alternation of muddy floodplain with sandy overbank and crevasse splay deposits associated with vertically stacked meandering channels. In the lower portion of these deposits, scattered plant remains, clay nodules and a pervasive silt and clayey silty matrix provide little evidence of pedogenesis (sample BP43; Figs 9 and 14J). Clay accumulation is, substantially, linked to infiltration processes occurring in permeable silty layers within the vadose zone, emplaced through overbank and crevasse processes during the periodic flood events (see also Ketzer *et al.*, 1999). These features suggest that repeated deposition and overbank and crevasse processes prevented the development of palaeosols (see also Milli *et al.*, 2016).

In the upper portion of the studied core (from 26 m upward), an abrupt increase of predominantly muddy units reflects a sudden drop in supply/accommodation ratio and a decrease in sedimentation rate (from 6.5 to 3.0 m kyr^{-1}). In this context, peat began to accumulate under a regime of rising groundwater and increasing accommodation, that facilitated the preservation of organic matter (as evidenced by organic-rich samples BP20, BP21, BP22, BP25, BP26 and BP27; Figs 9, 12 and 13). The base of the flood basin with swampy deposits is interpreted as a 'paludification surface (PaS)', (*sensu* Diessel *et al.*, 2000; Diessel, 2007). This surface shows pedogenetic features associated with faunal voids, excrement and plant remains (sample BP28), and is overlain by an organic-rich layer with a significant concentration of heavy metals (sample BP27). This diagnostic concentration in heavy metals (Cu, Ni) in the above layer, could be affected by many factors including organic matter content, sediment composition, pH condition and water saturation. In addition to plant activity, which exerts a significant effect on the availability of metals through the release of exudates from the roots, the presence of copper and nickel can be linked, for example, with the presence of organic matter (Alloway, 2012). Copper has a strong affinity for humic and fulvic acids and tends to naturally precipitate in Histosols (Alloway, 2012; Oorts, 2012). Another possible explanation for the presence of the heavy metals throughout the succession, could be related to the leaching of volcaniclastic alluvial material. The poorly stable phenocryst phases of volcaniclastic detritus (for example, pyroxene grains), may undergo rapid weathering during pedogenesis, releasing Ni and Cr metal concentrations in leaching groundwater that eventually precipitates within clay-rich intervals (Gonnelli & Renella, 2012).

Although a cursory examination of peaty horizons may link their formation to stagnant waters and stable reducing waterlogged conditions, micromorphological evidence from organic-rich floodplain deposits allows us to investigate in more detail the conditions of water saturation and pH during the organic layers formation. In particular, the stratigraphically lower flood basin with swampy deposits (26 to 21 m depth; Figs 5 and 9) are dominated by the presence of amorphous organic matter, calcareous nodules and gypsum precipitates (samples BP21, BP22, BP25 and BP26; Fig. 12M, N and O) that are indicators of neutral to moderately alkaline soils (pH 8.0 to 8.5). Conversely, up-section (from 21 to 16 m; Fig. 9), organic matter is associated with pyrite and siderite (samples BP16, BP17, BP18 and BP20; Fig. 13D, E and F) providing evidence for a reducing regime that became predominant during the formation of fibric and hemic horizons and is indicative of extremely acidic (pH 2.8 to 4.5) to near-neutral (pH 6.5 to 8.0) conditions with limited aeration (Retallack, 2001). Thus, the presence of interlayered sapric horizons within the flood basin with swampy facies associations, suggests that this sector of the alluvial plain experienced fluctuating oxidating regimes because of subaerial exposure and vertical groundwater variations. The sampled palaeosols at the top of the flood basin with swampy deposits (Figs 5 and 9) show carbonate impregnative features and gypsum precipitates that suggest relatively prolonged episodes of subaerial exposure and evapotranspiration processes (samples BP16 and BP18). This palaeosol couplet is separated by a charcoal-rich horizon (sample BP17 in Figs 9, 14M to O), which indicated that drought periods may have caused a lowering of water table allowing swamp fires.

Above the flood basin with swampy deposits, a drying-upward trend is recorded within the highstand deposits developed during the last 5 to 6 kyr. The HST deposits of the TDS developed when sea-level rise decreased reaching a relative stable position, and sediment bypassed leading to extensive seaward progradation (Milli *et al.*, 2016). Inland, the HST alluvial deposits host evidence of soil forming processes associated with precipitation of secondary carbonates and iron oxides (Fig. 14A, B, K and L). The HST alluvial deposits are, in fact,

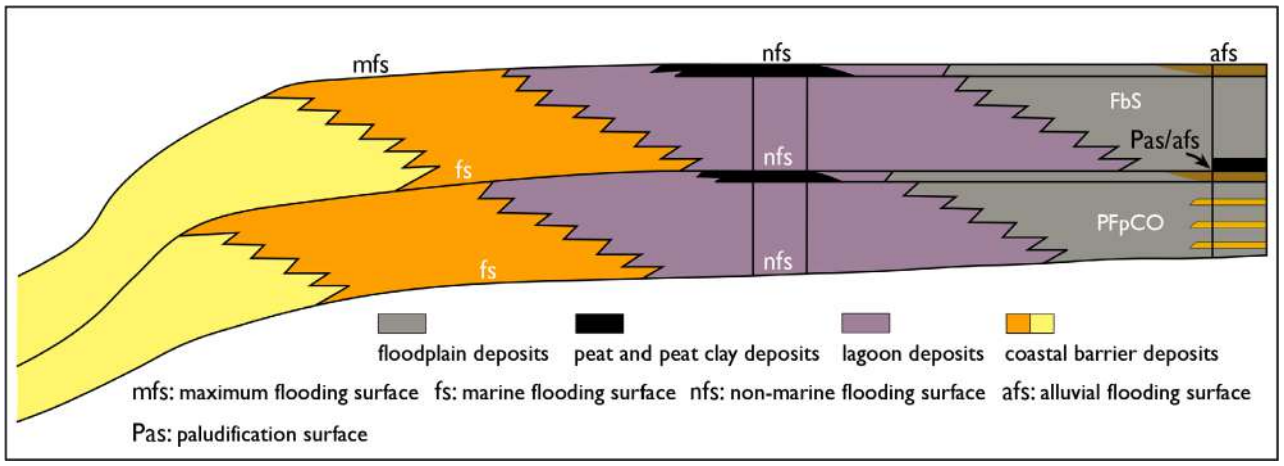

Fig. 18. Conceptual scheme showing the suggested physical correlation among the group of parasequences developed in the coastal, paralic/lagoon, and alluvial deposits constituting the transgressive systems tract (TST) of the Tiber Depositional Sequence (TDS). Not in scale.

characterized by incipient pedogenesis, owing to the slow aggradation rates and prolonged subaerial exposures. Such deposits are composed of indurated clay and silt with rare lignite layers, whereas carbonate-rich dry palaeosols with carbonate concretions, Fe/Mn oxide nodules and root traces are found frequently (samples BP5, BP6, BP7, BP8 and BP10; see also Milli *et al.*, 2016). Impregnative features and carbonate precipitation within the soil matrix are related to natural evapotranspiration and groundwater table fluctuation induced by the climatic variability. The formation of compound indurated soils acted as a natural barrier restricting water infiltration and leading to seasonal development of a perched water table. Such conditions favoured the occurrence of redox processes whose most common feature is represented by Fe nodules (Figs 14K, 14L and 15J to L).

The sequence-stratigraphic approach

The combination of sedimentological, micromorphological and compositional analyses allowed to characterize petrographic changes within the TST and HST alluvial deposits of the Tiber Depositional Sequence and across the main surfaces of sequence-stratigraphic significance. Considering that flooding surfaces related to single marine parasequences lacked physical expression in the floodplain deposits, the boundaries of groups of parasequences that were traced from coastal to alluvial environments within the TST and HST deposits of the TDS were recognized and tentatively correlated (Figs 4, 7 and 8).

In addition to the first transgressive and the maximum flooding surfaces, separating LST from TST and TST from HST, respectively, three main surfaces were recognized by using the detailed description of the BP well, constituting the landward expression of marine flooding surfaces in the paralic and floodplain deposits of the TST and HST, respectively (Fig. 4). In the lagoon/paralic deposits such surfaces correspond to the 'non-marine flooding surfaces' by Diessel *et al.* (2000) and occur on top of shallowing-upward lagoon units (parasequences) ending with peat layers (Fig. 18). In the alluvial deposits these surfaces, herein named 'alluvial flooding surfaces' (afs), occur on top of floodplain units with crevasse and overbank deposits which are characterized by incipient pedogenesis and at the base of peat layers (paludification surface by Diessel *et al.*, 2000) forming the initial deposits of organic-rich mud units (Fig. 18).

In the TST deposits, the alluvial flooding surface separates the FpCO from the PFpCO facies associations that are laterally associated with a series of vertically stacked active channel bodies with accreting side bars typical of a meandering channel (Figs 7 and 8); in the coastal sector this surface is placed at the top of the first group of parasequences of the TST (Fig. 4), which show a main aggradational and a subordinate retrogradational stacking pattern. Such a stacking pattern is coherent with the rate of sea-level rise that decreases to a value of 7.5 ± 1.1 mm year^{-1} due to the colder period of Younger Dryas (see Bard *et al.*, 2010). An alluvial marine flooding

surface also separates the PFpCO from the FbS facies associations. The PFpCO develops during an increase sea-level rise rate followed by a deceleration in the final phase of this facies association that could be related to the cold 8.2 yr BP event (Barber *et al.*, 1999; Clarke *et al.*, 2004). In the coastal sector this sedimentation phase shows a clear retrogradational stacking pattern of the second group of parasequences while the alluvial and floodplain deposits are characterized by FCh and floodplain aggradation, and record recurrent flood events through thick overbank and crevasse splay deposits. The final part of the PFpCO shows, locally, the presence of incipient palaeosols on top of which another alluvial flooding surface can be placed. The above organic-rich deposits mark the passage to the FbS facies association. On this basis, and taking into account the occurrence in these deposits of well-developed peat layers, the authors consider this alluvial flooding surface as the expression of the paludification surface by Diessel *et al.* (2000).

The FbS facies association suggests that such deposits formed during lower rates of sea-level and groundwater table rise and reflect processes that are accompanied by a greater stability of the alluvial and the coeval coastal/paralic environments, as evidenced by the sequence stratigraphic models developed by Kosters & Suter (1993), Bohacs & Suter (1997) and Tibert & Gibling (1999). In particular, the coeval deposits of FbS in the coastal/lagoon sector show an evident aggradational stacking pattern of two parasequences with peat layers developed in the back-barrier position (Milli *et al.*, 2016). This sector records the phase of maximum expansion of peatland that occurs just below the maximum flooding surface (Figs 4, 7 and 8). As evidenced by Diessel *et al.* (2000) the sedimentation rates of the peat layers are considerably lower than the associated clay deposits. Consequently, peat accumulation tends to form after the relative sea-level rise had decelerated to a rate that is compatible with the rate of peat formation. This is particularly evident in the TDS paralic/lagoon deposits (Milli *et al.*, 2016) where peat layers occur at the top of the depositional cycles constituting the landward expression of the coastal parasequences. In the alluvial deposits the FCh show marked amalgamation that reflects a reduction of the accommodation space. All of this is coherent with a deceleration of sea-level rise and with the changes of parasequence stacking pattern (from retrogradation/aggradation to progradation) that characterize the final phase of the TST and the beginning of the HST across the maximum flooding surface (see also Hamilton & Tadros, 1994; Flint *et al.*, 1995; Bohacs & Suter, 1997; Diessel, 2007; Wang *et al.*, 2019, 2020).

The top of the FbS facies association is marked by the maximum flooding surface above which WFp deposits occur. The latter formed during the HST of the TDS characterized by a slow rise in relative sea level which produced a slow alluvial plain aggradation of about 2.8 to 3.0 mm year^{-1}. An increase of sediment supply during the HST prevented the peat formation within these floodplain deposits, while the occurrence of dry palaeosols, rich in carbonate concretions, Fe/Mn oxide nodules, terrestrial gastropods and root traces suggest well-drained conditions.

These observations tell us about a specific history case of soil formation in an alluvial sector of the Tiber Depositional Sequence but may serve as a model to reconstruct the sequence-stratigraphic evolution of ancient relict soils. Nevertheless, additional criteria (for example, their stratigraphic position and correlative surfaces) are necessary to adequately interpret the genesis of such low-rank stratigraphic surfaces.

The analysis of the deposits from a petrographic point of view certainly defines the characters attributable to pedogenesis and palaeosol formation. However, it is also evident that the lack of a clear horizonation suggests incipient pedogenesis. These immature palaeosols are typified by very low compressive strength values (from 3 to <2 kg cm^{-2}) which may also suggest slight induration related to fluctuations in the groundwater levels. Nevertheless, although these immature palaeosols are discontinuous and have poor geotechnical properties the authors maintain that their use, from a sequence-stratigraphic point of view, can be made if framed in a robust sequence-stratigraphic scheme and where the physical relationships among depositional systems and systems tracts and the significance of the main stratigraphic surfaces are clear.

CONCLUSIONS

Depositional base level change and groundwater vertical movements influenced river sedimentation and the stacking pattern relationship among the facies associations developed in a selected sector of the Upper-Pleistocene/Holocene Tiber alluvial plain releasing an identifiable fingerprint on palaeosol surfaces. In particular, compositional

and micromorphological characterization of alluvial deposits developed within the transgressive systems tract (TST) and the highstand systems tract (HST) of the studied core suggests the following (from bottom to top):

1 Initial aggradation of fluvial channel (FCh) deposits prevented soil formation. Channel infill deposits show scattered plant remains and a pervasive silt and clayey silty matrix.

2 Slow but continuous sedimentation in the floodplain with crevasse and overbank deposits (FpCO) inhibited weathering and soil formation, although incipient pedogenesis has been recognized at the top of this facies association. This surface documents a palaeoenvironmental change from the FpCO to partially drained floodplain with crevasse and overbank (PFpCO) facies association. A weakly developed palaeosol documenting a partial subaerial exposure with bioturbation features and plant remains marks the passage from PFpCO to flood basin and swampy (FbS) facies association. This surface coincides with the paludification surface (PaS) and constitutes the base of the overlying peaty succession.

3 Within the FbS facies association the presence of multiple peat layers forming vertical stacked Histosols suggests increased waterlogging and flooding in response to a rising, although fluctuating, water table. Sulphide content within the peat can be associated with the presence of organic matter and may be related to the availability of sulphate in the groundwater. The top of this facies association is marked by a surface with a palaeosol couplet, characterized by encrusted roots, lignite remains, impregnative carbonate features and gypsum precipitates that document subaerial exposure; this surface represents the landward expression of the maximum flooding surface (mfs).

4 In the highstand deposits a periodical oxidative removal of plant material was observed because of increased microbial degradation and subaerial exposure during short-lived lowering of the water table. Such deposits are marked by incipient soil formation typified by iron oxides and carbonate precipitation. Iron nodule formation and carbonate translocation and precipitation are attributed to alternating wet and dry conditions. To explain the extensive overconsolidation within the uppermost portion of the HST deposits, precipitation of secondary carbonate released from soil solution leaching calcareous building debris from the above anthropogenic layer, may be envisaged.

In summary, the interpretation of pedogenetic features contextualized within a sequence-stratigraphic framework allowed to document changes in sediment composition and texture across stratigraphic surfaces of different genetic significance. Moreover, this study highlights that petrography and soil micromorphology can be used as a supporting tool to investigate the geotechnical characteristics of specific facies associations, which can be difficult to differentiate from cone penetration test (CPT) profiles or when using only grain-size criteria. However, care must be taken when expanding our results to similar alluvial settings, as CPT interpretation may not be relevant outside the local area.

In this study, one core is described in detail, but the authors emphasize that many of the facies associations and soil features described are common to the Tiber alluvial plain in the Rome urban area, providing a critical prerequisite for the understanding of the intrinsic characteristics of this urban soil.

ACKNOWLEDGEMENTS

This research was funded by Regione Lazio, FILAS project F87112000080007 "TIBER–Innovazione nel campo geotecnico per la definizione di strumenti, metodologie operative e procedure finalizzate alla realizzazione di un nuovo modello di sottosuolo (modello integrato)" project leader Francesco Stigliano and by the PetroSism Project (project coordinator Massimiliano Moscatelli). We are indebted to Francesca Trapasso for carrying out the X-ray diffraction analyses at the Institute of Environmental Geology and Geoengineering (IGAG) in Montelibretti and Domenico Mannetta for the thin section preparation at Sapienza, University of Rome. We thank Alessandro Amorosi and Luigi Bruno for their constructive feedback which has led to significant improvements of the manuscript and Editor Piret Plink-Björklund for her helpful and constructive comments.

REFERENCES

Acocella, V. and **Funiciello, R.** (2006) Transverse systems along the extensional Tyrrhenian margin of central Italy and their influence on volcanism. *Tectonics*, **25**, TC2003. https://doi.org/10.1020/2005TC001845

Adderley, P.W., **Wilson, C.A.**, **Simpson, I.A.** and **Davidson, D.A.** (2018) Anthropogenic features. In: *Interpretation of Micromorphological Features of Soils and Regoliths* (Eds Stoops, G., Marcellino, V. and Mees, F.), pp. 753–777. Elsevier, Amsterdam.

Adderley, W.P., **Wilson, C.A.**, **Simpson, I.A.** and **Davidson, D.A.** (2010) Anthropogenic features. In: *Interpretation of Micromorphological Features of Soils and Regoliths* (Eds Stoops, G., Marcelino, V. and Mees, F.), pp. 569–588. Elsevier, Amsterdam.

Allen, P.A. (2008) Time scales of tectonic landscapes and their sediment routing systems. In: *Special Publication Geological Society London, Earth's Dynamic Surface: Catastrophe and Continuity in Landscape Evolution* (Eds Gallagher, K., Jones, S.J. and Wainwright, J.), *Geol. Soc. Spec. Publ.*, **296**, 7–28.

Alloway, B.J. (2012) Heavy metals in soils: trace metals and metalloids in soils and their bioavailability. In: *Heavy Metals in Soils: Trace Metals and Metalloids in Soils and Their Bioavailability, Environmental Pollution* (Ed. Alloway, B.J.), vol. **22**, pp. 11–50. Springer, Dordrecht.

Amorosi, A., **Bruno, L.**, **Cleveland, D.M.**, **Morelli, A.** and **Hong, W.** (2017) Paleosols and associated channel-belt sand bodies from a continuously subsiding late quaternary system (Po Basin, Italy): new insights into continental sequence stratigraphy. *Bull. Geol. Soc. Am.*, **129**, 449–463.

Amorosi, A., **Bruno, L.**, **Campo, B.**, **Costagli, B.**, **Hong, W.**, **Picotti, V.** and **Vaiani, S.C.** (2021) Deformation patterns of upper Quaternary strata and their relation to active tectonics, Po Basin, Italy. *Sedimentology*, **68**, 402–424.

Amorosi, A. and **Marchi, N.** (1999) High-resolution sequence stratigraphy from piezocone tests: an example from the Late Quaternary deposits of the southeastern Po Plain. *Sediment. Geol.*, **128**, 67–81.

Amorosi, A. and **Zuffa, G.G.** (2011) Sand composition changes across key boundaries of siliciclastic and hybrid depositional sequences. *Sediment. Geol.*, **236**, 153–163.

Aslan, A. and **Autin, W.J.** (1996) Depositional and pedogenic influences on the environmental geology of Holocene Mississippi River floodplain deposits near Ferriday. *Louisiana. Eng. Geol.*, **45**, 417–432.

Barber, D.C., **Dyke, A.**, **Hillaire-Marcel, C.**, **Jennings, A.E.**, **Andrews, J.T.**, **Kerwin, M.W.**, **Bilodeau, G.**, **McNeely, R.**, **Southon, J.**, **Morehead, M.D.** and **Gagnon, J.M.** (1999) Forcing of the cold event of 8,200 years ago by catastrophic drainage of Laurentide lakes. *Nature*, **400**, 344–348.

Bard, E., **Hamelin, B.** and **Delanghe-Sabatier, D.** (2010) Deglacial meltwater pulse 1B and Younger Dryas sea levels revisited with boreholes at Tahiti. *Science*, **327**, 1235–1237.

Bellotti, P., **Chiocci, F.L.**, **Milli, S.**, **Tortora, P.** and **Valeri, P.** (1994) Sequence stratigraphy and depositional setting of the Tiber delta: integration of high-resolution seismics, well logs, and archeological data. *J. Sed. Res.*, **B64**, 416–432.

Bellotti, P., **Milli, S.**, **Tortora, P.** and **Valeri, P.** (1995) Physical stratigraphy and sedimentology of the late Pleistocene-Holocene Tiber Delta depositional sequence. *Sedimentology*, **42**, 617–634.

Blott, S.J. and **Pye, K.** (2012) Particle size scales and classification of sediment types based on particle size distributions: review and recommended procedures. *Sedimentology*, **59**, 2071–2096.

Blum, M., **Martin, J.**, **Milliken, K.** and **Garvin, M.** (2013) Paleovalley systems: insights from quaternary analogs and experiments. *Earth-Sci. Rev.*, **116**, 128–169.

Blum, M.D. and **Price, D.M.** (1998) Quaternary alluvial plain construction in response to glacio-eustatic and climatic controls, Texas Gulf coastal plain. In: *Relative Role of Eustasy, Climate, and Tectonism in Continental Rocks* (Eds Shanley, K.W. and McCabe, P.J.), *Spec. Publ. Soc. Econ. Paleont. Miner.*, **59**, 31–48.

Blum, M.D., **Toomey III, R.S.** and **Valastro Jr., S.** (1994) Fluvial response to Late Quaternary climatic and environmental change, Edwards Plateau, Texas. *Palaeogeogr. Palaeoclimatol. Palaeoecol.*, **108**, 1–21.

Blum, M.D. and **Törnqvist, T.E.** (2000) Fluvial responses to climate and sea-level change: a review and look forward. *Sedimentology*, **47**, 2–48.

Bohacs, K. and **Suter, J.** (1997) Sequence stratigraphic distribution of coaly rocks: fundamental controls and paralic examples. *Am. Asso. Petrol. Geol. Bull.*, **81**, 1612–1639.

Bordoni, P. and **Valensise, G.** (1998) Deformation of the 125 ka marine terrace in Italy: tectonic implications. In: *Late Quaternary Coastal Tectonics* (Eds Stewart, I. and Vita-Finzi, C.), *Geol. Soc. London, Spec. Publ.*, **146**, 71–110.

Bozzano, F., **Andreucci, A.**, **Gaeta, M.** and **Salucci, R.** (2000) A geological model of the buried Tiber River valley beneath the historical centre of Rome. *Bull. Eng. Geol. Environ.*, **59**, 1–21.

Bozzano, F., **Caserta, A.**, **Govoni, A.**, **Marra, F.** and **Martino, S.** (2008) Static and dynamic characterization of alluvial deposits in the Tiber River Valley: new data for assessing potential ground motion in the City of Rome. *J. Geophys. Res. Solid Earth*, **113**, 1–21.

Bridge, J.S. and **Demicco, R.V.** (2008) *Earth Surface Processes, Landforms and Sediment Deposits*. Cambridge University Press, Cambridge, 815 pp.

Bullock, P., **Fedoroff, N.**, **Jongerius, A.**, **Stoops, G.** and **Tursina, T.** (1985) *Handbook for Soil Thin Section Description*. Waine Research, Wolverampthon, 152 pp.

Buol, S.W., **Southard, R.J.**, **Graham, R.C.** and **McDaniel, P.A.** (2011) In: *Soil Genesis and Classification* (Eds Buol, S.W., Southard, R.J., Graham, R.C. and McDaniel, P.A.). John Wiley & Sons, Chichester, 543 pp.

Cai, G., **Puppala, A.J.** and **Liu, S.** (2014) Characterization on the correlation between shear wave velocity and piezocone tip resistance of Jiangsu clays. *Eng. Geol.*, **171**, 96–103.

Catuneanu, O., **Abreu, V.**, **Bhattacharya, J.P.**, **Blum, M.D.**, **Dalrymple, R.W.**, **Eriksson, P.G.**, **Fielding, C.R.**, **Fisher, W.L.**, **Galloway, W.E.** and **Gibling, M.R.** (2009) Towards the standardization of sequence stratigraphy. *Earth-Sci. Rev.*, **92**, 1–33.

Catuneanu, O., **Galloway, W.E.**, **Kendall, C.G.S.C.**, **Miall, A.D.**, **Posamentier, H.W.**, **Strasser, A.** and **Tucker, M.E.** (2011) Sequence stratigraphy: methodology and nomenclature. *Newslett. Stratigr.*, **44**, 173–245.

Cavinato, G.P., **De Rita, D.**, **Milli, S.** and **Zarlenga, F.** (1992) Correlazione tra I principali eventi tettonici, sedimentari, vulcanici ed eustatici che hanno interessato l'entroterra (conche intrappenniniche) e il margine costiero tirrenico laziale durante il Pliocene Superiore ed il Pleistocene, Vol. *Spec. Studi Geol. Camerti.*, **1**, 109–114.

Charpentier, D., **Cathelineau, M.**, **Mosser-Ruck, R.** and **Bruno, G.** (2001) Mineralogical evolution of argilites in dehydrated-oxidised zones: the example of the argilitic walls from Tournemire tunnel. *Comptes Rendus L'academie Des Sci. Ser. 2a, Sci. La Terre Des Planetes*, **332**, 601–607.

Chow, T.J. and **Goldberg, E.D.** (1960) On the marine geochemistry of barium. *Geochim. Cosmochim. Acta*, **20**, 192–198.

Clarke, G.K., **Leverington, D.W.**, **Teller, J.T.** and **Dyke, A.S.** (2004) Paleohydraulics of the last outburst flood from glacial Lake Agassiz and the 8200 BP cold event. *Quatern. Sci. Rev.*, **23**, 389–407.

Conato, V., **Esu, D.**, **Malatesta, A.** and **Zarlenga, F.** (1980) New data on the Pleistocene of Rome. *Quaternaria*, **22**, 131–176.

Courty, M.-A. and **Fedoroff, N.** (1985) Micromorphlogy of recent and buried soils in a semi-arid region of northwestern India. *Geoderma*, **35**, 287–332.

De Rita, D., **Fabbri, M.**, **Mazzini, I.**, **Paccara, P.**, **Sposato, A.** and **Trigari, A.** (2002) Volcaniclastic sedimentation in coastal environments: the interplay between volcanism and Quaternary sea level changes (central Italy). *Quat. Int.*, **95**, 141–154.

De Rita, D., **Faccenna, C.**, **Funiciello, R.** and **Rosa, C.** (1995) Stratigraphy and volcano-tectonics. In: *The Volcano of the Alban Hills* (Ed. Trigila, R.), Tipografia S.G.S, Roma, 33–71.

De Rita, D., **Funiciello, R.**, **Corda, L.**, **Sposato, A.** and **Rossi, U.** (1993) Volcanic unit. In: *Sabatini Volcanic Complex* (Ed. Di Filippo, M.), Consiglio Nazionale Delle Ricerche, Progetto Finalizzato "Geodinamica" Monografie Finali, **11**, 33–79.

Di Salvo, C., **Mancini, M.**, **Cavinato, G.P.**, **Moscatelli, M.**, **Simionato, M.**, **Stigliano, F.**, **Rea, R.** and **Rodi, A.** (2020) A 3D geological model as a base for the development of a conceptual groundwater scheme in the area of the colosseum (Rome, Italy). *Geosciences*, **10**, 266.

Diessel, C.F.K. (2007) Utility of coal petrology for sequence-stratigraphic analysis. *Int. J. Coal Geol.*, **70**, 3–34.

Diessel, C., **Boyd, R.**, **Wadsworth, J.**, **Leckie, D.** and **Chalmers, G.** (2000) On balanced and unbalanced accommodation/peat accumulation ratios in the Cretaceous coals from Gates Formation, Western Canada, and their sequence-stratigraphic significance. *Int. J. Coal Geol.*, **43**, 143–186.

Doglioni, C., **Innocenti, F.**, **Morellato, C.**, **Procaccianti, D.** and **Scrocca, D.** (2004) On the Tyrrhenian sea opening. *Mem. Descr. Carta. Geol. D'it.*, **64**, 147–164.

Esteban, M. and **Klappa, C.F.** (1983) Subaerial exposure environment. In: *Carbonate Depositional Environments* (Eds Scholle, P.A., Bebout, D.G. and Moore, C.H.), *Assoc. Am. Petr. Geol. Mem.*, **33**, 1–54.

Fear, C.E. and **Robertson, P.K.** (1995) Estimating the undrained strength of sand: a theoretical framework. *Can. Geotech. J.*, **32**, 859–870.

Fedoroff, N., **Courty, M.-A.** and **Guo, Z.** (2010) Palaeosoils and relict soils. In: *Interpretation of Micromorphological Features of Soils and Regoliths* (Eds Stoops, G., Marcellino, V. and Mees, F.), pp. 623–662. Elsevier, Amsterdam.

Flint, S., **Aitken, J.** and **Hampson, G.** (1995) Application of sequence stratigraphy to coal-bearing coastal plain successions: implications for the UK Coal Measures. In: *European Coal Geology* (Eds Whateley, M.K.G. and Spears, D.A.), *Geological Society, London, Special Publications*, **82**, 1–16.

Fornaseri, M. (1985) Geochronology of volcanic rocks from Lazio (Italy). *Rend. Soc. Ital. Min. Petr.*, **40**, 73–106.

Gasparatos, D. (2012) Fe–Mn concretions and nodules to sequester heavy metals in soils. In: *Environmental Chemistry for a Sustainable World* (Eds Licthfouse, E., Schwarzbauer, J. and Robert, D.), pp. 443–474. Springer, Berlin.

Giordano, G., **Esposito, A.**, **De Rita, D.**, **Fabbri, M.**, **Mazzini, I.**, **Trigari, A.**, **Rosa, C.** and **Funiciello, R.** (2003) The sedimentation along the roman coast between middle and Upper Pleistocene: the interplay of eustatism, tectonics and volcanism-new data and review. *Quaternario*, **16**, 121–129.

Gonnelli, C. and **Renella, G.** (2012) Key heavy metals and metalloids – chromium and nickel. In: *Heavy Metals in Soils: Trace Metals and Metalloids in Soils and Their Bioavailability, Environmental Pollution* (Ed. Alloway, B.J.), vol. **22**, pp. 313–333. Springer, Dordrecht.

Hamilton, D.S. and **Tadros, N.Z.** (1994) Utility of coal seams as genetic stratigraphic sequence boundaries in nonmarine basins: an example from the Gunnedah Basin, Australia. *Am. Asso. Petrol. Geol. Bull.*, **78**, 267–286.

Holz, M., **Kalkreuth, W.** and **Banerjee, I.** (2002) Sequence stratigraphy of paralic coal-bearing strata: an overview. *Int. J. Coal Geol.*, **48**, 147–179.

Horne, J.C., **Ferm, J.C.**, **Caruccio, F.T.** and **Baganz, B.P.** (1978) Depositional models in coal exploration and mine planning in Appalachian region. *Am. Assoc. Pet. Geol. Bull.*, **62**, 2379–2411.

Husseiny, A.E. and **Vanorio, T.** (2015) The effect of micrite content on the acoustic velocity of carbonate rocks. *Geophysics*, **80**, L45–L55.

Ingersoll, R.V., **Bullard, T.F.**, **Ford, R.L.**, **Grimm, J.P.**, **Pickle, J.D.** and **Sares, S.W.** (1984) The effect of grain size on detrital modes: a test of the Gazzi-Dickinson point-counting method. *J. Sediment. Res.*, **54**, 103–116.

Itkin, D., **Goldfus, H.** and **Monger, H.C.** (2016) Human induced calcretisation in anthropogenic soils and sediments: field observations and micromorphology in a Mediterranean climatic zone, Israel. *Catena*, **146**, 48–61.

Jerrett, R.M., **Flint, S.S.**, **Davies, R.C.** and **Hodgson, D.M.** (2011) Sequence stratigraphic interpretation of a Pennsylvanian (Upper Carboniferous) coal from the central Appalachian Basin, USA. *Sedimentology*, **58**, 1180–1207.

Jim, C.Y. (1998) Urban soil characteristics and limitations for landscape planting in Hong Kong. *Landsc. Urban Plan*, **40**, 235–249.

Kazemian, S. (2015) Effect of different binders on settlement of fibrous peat. *Soil Mech. Found. Eng.*, **52**, 9–14.

Kemp, R.A. (1995) Distribution and genesis of calcitic pedofeatures within a rapidly aggrading loess-paleosol sequence in China. *Geoderma*, **65**, 303–316.

Kenter, J.A.M., **Braaksma, H.**, **Verwer, K.** and **van Lanen, X.M.T.** (2007) Acoustic behavior of sedimentary rocks: Geologic properties versus poisson's ratios. *Lead. Edge*, **26**, 436–444.

Ketzer, J.M., **Morad, S.** and **Amorosi, A.** (1999) Predictive diagenetic clay-mineral distribution in siliciclastic rocks within a sequence stratigraphic framework. In: *Clay Mineral Cements in Sandstones* (Eds Worden, R.H. and Morad, S.), *Int. Ass. Sed. Spec. Publ.*, **34**, 43–61.

Klappa, C.F. (1980) Rhizoliths in terrestrial carbonates: classification, recognition, genesis and significance. *Sedimentology*, **27**, 613–629.

Kooistra, M.J. and **Pulleman, M.M.** (2010) Features related to faunal activity. In: *Interpretation of Micromorphological Features of Soils and Regoliths* (Eds Stoops, G., Marcellino, V. and Mees, F.), pp. 397–418. Elsevier, Amsterdam.

Kosters, E.C. and **Suter, J.R.** (1993) Facies relationships and systems tracts in the late Holocene Mississippi delta plain. *J. Sediment. Res.*, **63**, 727–733.

Kostova, I. and **Zdravkov, A.** (2007) Organic petrology, mineralogy and depositional environment of the Kipra lignite seam, Maritza-West basin, Bulgaria. *Int. J. Coal Geol.*, **71**, 527–541.

Kraus, M.J. (1987) Integration of channel and floodplain suites; II, Vertical relations of alluvial Paleosols. *J. Sediment. Res.*, **57**, 602–612.

Kraus, M.J. and **Aslan, A.** (1993) Eocene hydromorphic Paleosols: significance for interpreting ancient floodplain processes. *J. Sediment. Res.*, **63**, 453–463.

Locardi, E., **Lombardi, G.**, **Funiciello, R.** and **Parotto, M.** (1976) The main volcanic group of Lazio (Italy): relations between structural evolution and petrogenesis. *Geol. Romana*, **15**, 279–300.

Maffucci, R., **Ciotoli, G.**, **Pietrosante, A.**, **Cavinato, G.P.**, **Milli, S.**, **Ruggiero, L.**, **Sciarra, A.** and **Bigi, S.** (2022) Geological hazard assessment of the coastal area of Rome (central Italy) from multi-source data integration. *Eng. Geol.* in press. https://doi.org/10.1016/j.enggeo.2022.106527

Malinverno, A. and **Ryan, W.B.F.** (1986) Extension in the Tyrrhenian Sea and shortening in the Apennines as result of arc migration driven by sinking of the lithosphere. *Tectonics*, **5**, 227–245.

Mancini, M. and **Cavinato, G.P.** (2005) The middle valley of the Tiber River, Central Italy: Plio-Pleistocene fluvial and coastal sedimentation, extensional tectonics and volcanism. In: *Fluvial Sedimentology VII* (Eds Blum, M.D., Marriott, S.B. and Leclair, S.F.), IAS Spec. Publ., **35**, 373–396.

Mancini, M., **D'Anastasio, E.**, **Barbieri, M.** and **De Martini, P.M.** (2007) Geomorphological, paleontological and 87Sr/86Sr isotope analyses of early Pleistocene paleoshorelines to define the uplift of Central Apennines (Italy). *Quat. Res.*, **67**, 487–501.

Mancini, M., **Moscatelli, M.**, **Stigliano, F.**, **Cavinato, G.P.**, **Marini, M.**, **Pagliaroli, A.** and **Simionato, M.** (2013a) Fluvial facies and stratigraphic architecture of Middle Pleistocene incised valleys from the subsoil of Rome (Italy). *J. Mediterr. Earth Sci.*, **5**, 89–93.

Mancini, M., **Moscatelli, M.**, **Stigliano, F.**, **Cavinato, G.P.**, **Milli, S.**, **Pagliaroli, A.**, **Simionato, M.**, **Brancaleoni, R.**, **Cipolloni, I.**, **Coen, G.**, **Di Salvo, C.**, **Garbin, F.**, **Lanzo, G.**, **Napoleoni, Q.**, **Scarapazzi, M.**, **Storoni Ridolfi, S.** and **Vallone, R.** (2013b) The Upper Pleistocene-Holocene fluvial deposits of the Tiber River in Rome (Italy): lithofacies, geometries, stacking pattern and chronology. *J. Mediterr. Earth Sci.*, **5**, 95–101.

Marcelino, V., **Schaefer, C.E.G.R.** and **Stoops, G.** (2018) Oxic and related materials. In: *Interpretation of micromorphological features of soils and regoliths* (Eds Stoops, G., Marcellino, V. and Mees, F.), pp. 663–689. Elsevier, Amsterdam.

McCabe, P.J. (1985) Depositional environments of coal and coal-bearing strata. *Sedimentol. Coal Coal-Bearing Seq.*, **7**, 11–42.

McCarthy, P.J., **Martini, I.P.** and **Leckie, D.A.** (1998) Use of micromorphology for palaeoenvironmental interpretation of complex alluvial palaeosols: an example from the Mill Creek Formation (Albian), southwestern Alberta, Canada. *Palaeogeogr. Palaeoclimatol. Palaeoecol.*, **143**, 87–110.

McCarthy, P.J. and **Plint, A.G.** (1998) Recognition of interfluve sequence boundaries: integrating paleopedology and sequence stratigraphy. *Geology*, **26**, 387–390.

Milli, S. (1994) High-frequency sequence stratigraphy of the middle-late Pleistocene to Holocene deposits of the Roman Basin (Rome, Italy): relationships among high frequency eustatic cycles, tectonics and volcanism. *Second High-Resolution Sequence Stratigraphy Conference* (Eds Posamentier, H.W. and Mutti, E.), pp. 20–27. Tremp, Spain.

Milli, S. (1997) Depositional setting and high-frequency sequence stratigraphy of the Middle-Upper Pleistocene to Holocene deposits of the Roman Basin. *Geol. Rom.*, **33**, e136.

Milli, S., **D'Ambrogi, C.**, **Bellotti, P.**, **Calderoni, G.**, **Carboni, M.G.**, **Celant, A.**, **Di Bella, L.**, **Di Rita, F.**, **Frezza, V.**, **Magri, D.**, **Pichezzi, R.M.** and **Ricci, V.** (2013) The transition from wave-dominated estuary to wave-dominated delta: the Late Quaternary stratigraphic architecture of Tiber River deltaic succession (Italy). *Sediment. Geol.*, **284**, 159–180.

Milli, S., **Mancini, M.**, **Moscatelli, M.**, **Stigliano, F.**, **Marini, M.** and **Cavinato, G.P.** (2016) From river to shelf, anatomy of a high-frequency depositional sequence: The Late Pleistocene to Holocene Tiber depositional sequence. *Sedimentology*, **63**, 1886–1928.

Milli, S., **Moscatelli, M.**, **Palombo, M.R.**, **Parlagreco, L.** and **Paciucci, M.** (2008) Incised-valleys, their filling and mammal fossil record: a case study from Middle-Upper Pleistocene deposits of the Roman Basin (Latium, Italy). *Adv. Appl. Seq. Stratigr. Italy GeoActa, Spec. Publ.*, **1**, 667–687.

Mitchell, J.K. and **Kenichi, S.** (2005) Time effects on strength and deformation. In *Fundamentals of Soil Behaviour* (Eds Mitchell, J.K. and Soga, K.), pp. 465–522.

Mitchum Jr., R.M. and **Van Wagoner, J.C.** (1991) High-frequency sequences and their stacking patterns: sequence-stratigraphic evidence of high-frequency eustatic cycles. *Sediment. Geol.*, **70**, 131–160.

Moormann, F.R. and **Eswaran, H.** (1978) A study of a Paleosol from East Nigeria. *Pedologie*, **28**, 251–270.

Nirei, H., **Mezzano, A.**, **Satkunas, J.**, **Furuno, K.**, **Marker, B.** and **Mitamura, M.** (2014) Environmental problems associated with man-made strata and their potential management. *Episodes J. Int. Geosci.*, **37**, 33–40.

Oorts, K. (2012) Key heavy metals and metalloids – copper. In: *Heavy Metals in Soils: Trace Metals and Metalloids in Soils and Their Bioavailability, Environmental Pollution* (Ed. Alloway, B.J.), vol. **22**, pp. 367–394. Springer, Dordrecht.

Ou, Z.F. and **Fang, Y.G.** (2017) The influence of organic matter content on the rheological model parameters of soft clay. *Soil Mech. Found. Eng.*, **54**, 283–288.

Patacca, E., **Sartori, R.** and **Scandone, P.** (1990) Tyrrhenian basin and Apenninic arcs: kinematic relations since late Tortonian times. *Mem. Della Soc. Geol. Ital.*, **45**, 425–451.

Peccerillo, A. (2005) *Plio-Quaternary Volcanism in Italy*, p. 365. Springer, Berlin.

Poch, R.M., **Artieda, O.** and **Lebedeva, M.** (2018) Gypsic features. In: *Interpretation of Micromorphological Features of Soils and Regoliths* (Eds Stoops, G., Marcellino, V. and Mees, F.), pp. 259–287. Elsevier, Amsterdam.

Prokof'eva, T., **Sedov, S.N.**, **Stroganova, M.N.** and **Kazdym, A.A.** (2001) An experience of the micromorphological diagnostics of urban soils. *Eurasian Soil Sci.*, **34**, 783–792.

Prokof'eva, T., **Shishkov, V.** and **Kiriushin, A.** (2020) Calcium carbonate accumulations in Technosols of Moscow city. *J. Soils Sed.*, **21**, 2049–2058. https://doi.org/10.1007/s11368-020-02696-y

Prokof'eva, T., **Umarova, A.**, **Bykova, G.**, **Suslenkova, M.**, **Ezhelev, Z.**, **Kokoreva, A.**, **Gasina, A.** and **Martynenko, I.** (2021) Morphological and physical properties in diagnostics of urban soils: case study from Moscow, Russia. *Soil Sci. Annu.*, **71**, 309–320. https://doi.org/10.37501/soilsa/131598

Rabenhorst, M.C. and **Haering, K.C.** (1989) Soil micromorphology of a Chesapeake Bay tidal marsh: implications for sulfur accumulation. *Soil Sci.*, **147**, 339–347.

Rabenhorst, M.C. and **James, B.R.** (1992) Iron sulfidization in tidal marsh soils. *Catena. Suppl.*, 203–217.

Retallack, G.J. (Ed.). (2001) *Soils of the Past: An Introduction to Paleopedology*, 2nd edn. Blackwell Science, Oxford, 404 pp.

Rita, D.E., **Milli, S.**, **Rosa, C.**, **Zarlenga, F.** and **Cavinato, G.P.** (1994) Catastrophic eruptions and eustatic cycles: example of Latium volcanoes. *Atti Dei Convegni Lincei, Acc. Naz. Lin*, **112**, 135–142.

Romans, B.W., **Castelltort, S.**, **Covault, J.A.**, **Fildani, A.** and **Walsh, J.P.** (2016) Environmental signal propagation in sedimentary systems across timescales. *Earth-Sci. Rev.*, **153**, 7–29.

Sarti, G., **Rossi, V.** and **Amorosi, A.** (2012) Influence of Holocene stratigraphic architecture on ground surface settlements: a case study from the City of Pisa (Tuscany, Italy). *Sediment. Geol.*, **281**, 75–87.

Schleuß, U., **Wu, Q.** and **Blume, H.P.** (1998) Variability of soils in urban and periurban areas in Northern Germany. *Catena*, **33**, 255–270.

Sehgal, J.L. and **Stoops, G.** (1972) Pedogenic calcite accumulation in arid and semi-arid regions of the Indo-Gangetic alluvial plain of erstwhile Punjab (India)—their morphology and origin. *Geoderma*, **8**, 59–72.

Srivastava, P., **Rajak, M.K.**, **Sinha, R.**, **Pal, D.K.** and **Bhattacharyya, T.** (2010) A high-resolution micromorphological record of the Late Quaternary paleosols from Ganga-Yamuna interfluve: stratigraphic and paleoclimatic implications. *Quat. Int.*, **227**, 127–142.

Srivastava, P., **Sinha, R.**, **Deep, V.**, **Singh, A.** and **Upreti, N.** (2018) Micromorphology and sequence stratigraphy of the interfluve paleosols from the Ganga Plains: a record of alluvial cyclicity and paleoclimate during the Late Quaternary. *J. Sediment. Res.*, **88**, 105–128.

Staff, S.S. (2014) *Keys to Soil Taxonomy*, 12th edn. Department of Agriculture (USDA) Natural Resources Conservation Service (NRCS), Washington, DC.

Stolt, M.H. and **Lindbo, D.L.** (2010) Soil organic matter. In: *Interpretation of Micromorphological Features of Soils and Regoliths* (Eds Stoops, G., Marcellino, V. and Mees, F.), pp. 369–396. Elsevier, Amsterdam.

Stoops, G. (Ed.). (2021) *Guidelines for Analysis and Description of Soil and Regolith Thin Sections*. John Wiley & Sons, Oxford, 256pp.

Stoops, G., **Marcelino, V.** and **Mees, F.** (Eds). (2018) *Interpretation of Micromorphological Features of Soils and Regoliths*, 2nd Ed. Elsevier, Amsterdam, 1000 p.

Stoops, G.J. and **Zavaleta, A.** (1978) Micromorphological evidence of barite neoformation in soils. *Geoderma*, **20**, 63–70.

Styllas, M. (2014) A simple approach to define Holocene sequence stratigraphy using borehole and cone penetration test data. *Sedimentology*, **61**, 444–460.

Szymański, W. and **Skiba, M.** (2013) Distribution, morphology, and chemical composition of Fe-Mn nodules in Albeluvisols of the Carpathian Foothills, Poland. *Pedosphere*, **23**, 445–454.

Tentori, D., **Amorosi, A.**, **Milli, S.** and **Marsaglia, K.M.** (2021) Sediment dispersal pathways in the Po coastal plain since the Last Glacial Maximum: provenance signals of autogenic and eustatic forcing. *Basin Res.*, **33**, 1407–1428.

Tentori, D., **Marsaglia, K.M.** and **Milli, S.** (2016) Sand compositional changes as a support for sequence-Stratigraphic interpretation: the middle upper Pleistocene to Holocene deposits of the roman basin (Rome, Italy). *J. Sediment. Res.*, **86**, 1208–1227.

Tentori, D., **Milli, S.** and **Marsaglia, K.M.** (2018) A source-to-sink compositional model of a present highstand: an example in the low-rank Tiber depositional sequence (Latium tyrrhenian margin, Italy). *J. Sediment. Res.*, **88**, 1238–1259.

Tibert, N.E. and **Gibling, M.R.** (1999) Peat accumulation on a drowned coastal braidplain: the Mullins Coal (Upper Carboniferous), Sydney Basin, Nova Scotia. *Sed. Geol.*, **128**, 23–38.

Vepraskas, M.J., **Lindbo, D.L.** and **Lin, H.** (2012) Redoximorphic features as related to soil hydrology and hydric soils. In: *Hydropedology Synergistic Integration of Soil Science and Hydrology* (Ed. Lin, H.), pp. 143–172. Academic Press, San Diego.

Vissac, C. (2005) Study of a historical garden soil at the Grand-Pressigny site (Indre-et-Loire, France): evidence of landscape management. *J. Cult. Herit.*, **6**, 61–67.

Wada, H. and **Seisuwan, B.** (1986) The process of pyrite formation in mangrove soils. In: *Selected Papers of the Dakar Symposium on Acid Sulphate Soils* (Ed Dost, H.). *Dakar*, **44**, 24–37.

Wang, S., **Shao, L.**, **Wang, D.**, **Sun, Q.**, **Sun, B.** and **Lu, J.** (2019) Sequence stratigraphy and coal accumulation of Lower Cretaceous coal-bearing series in Erlian Basin, Northeastern China. *Am. Asso. Petrol. Geol. Bull.*, **103**, 1653–1690.

Wang, S., **Shao, L.**, **Wang, D.**, **Hilton, J.**, **Guo, B.** and **Lu, J.** (2020) Controls on accumulation of anomalously thick coals: Implications for sequence stratigraphic analysis. *Sedimentology*, **67**, 991–1013.

Wieder, M. and **Yaalon, D.H.** (1982) Micromorphological fabrics and developmental stages of carbonate nodular forms related to soil characteristics. *Geoderma*, **28**, 203–220.

Yamnova, I.A. and **Pankova, E.I.** (2013) Gypsic pedofeatures and elementary pedogenetic processes of their formation. *Eurasian Soil Sci.*, **46**, 1117–1129.

Zuffa, G.G., **Cibin, U.** and **Di Giulio, A.** (1995) Arenite petrography in sequence stratigraphy. *J. Geol.*, **103**, 451–459.

Zuffetti, C., **Trombino, L.**, **Zembo, I.** and **Bersezio, R.** (2018) Soil evolution and origin of landscape in a late Quaternary tectonically mobile setting: The Po Plain-Northern Apennines border in Lombardy (Italy). *Catena*, **171**, 376–397.

Manuscript received 12 June 2021; revision accepted 14 December 2021

Supporting Information

Additional information may be found in the online version of this article:

Fig S1. Examples of bioclast remains in poorly drained and pedogenized floodplain deposits.

Fig S2. Energy-dispersive X-ray spectroscopy (EDS) spectra of authigenic minerals and heavy metals.

Table S1. Counted and recalculated parameters.

Table S2. Point-count data and detrital modes.